Review of Materials Research 1 (2025) 100012

Contents lists available at ScienceDirect

Review of Materials Research

journal homepage: www.sciencedirect.com/journal/review-of-materials-research

Electrolyte modulation strategies towards cathode-electrolyte interphase engineering in subzero-temperature lithium-ion batteries

Zihan Xiong, Fanbo Meng, Jiahe Chen, Zhenzhong Yang, Renzong Hu *, Min Zhu

School of Materials Science and Engineering, Guangdong Provincial Key Laboratory of Advanced Energy Storage Materials, South China University of Technology, Guangzhou, 510640, China

ARTICLE INFO

Keywords:
Low-temperature performance
Cathode-electrolyte interface
Electrolyte modulation
Layered oxide cathode
Electrochemical kinetics reaction

ABSTRACT

Failure of lithium-ion batteries (LIBs) under subfreezing conditions limits their further development in aerospace and military applications, including severe capacity degradation, poor charge ability, and safety issue. Sluggish electrochemical reaction kinetics in the cathode-electrolyte interphases (CEI) would restrict the diffusion transfer of electric charge and Li^+ ions, which is regarded as the main factor contributing to the low-temperature electrochemical failure issue. This review introduces and discusses the latest important interfacial CEI engineering on the layered oxide cathode in enhancing the low-temperature performance of LIBs based on the electrolyte modulation strategies. Firstly, the interfacial issues of layered oxide cathodes and the formation mechanism of CEI film under subzero temperatures are introduced. Secondly, recent progress about the interfacial engineering on inducing CEI construction under low temperature is summarized in terms of the components mainly involved in anions of Li salt, solvent molecule and additive. Thirdly, considering the unique composition and structure of CEI films, advanced interfacial characterization techniques and analysis are summarized. Finally, a perspective of electrolyte design matched with layered cathode materials in low-temperature LIBs is further presented, which may supply a new sight into designs and manufacture of LIBs and other devices for subzero-temperature applications.

1. Introduction

Lithium-ion batteries (LIBs) and related electric devices have emerged as the predominant electrochemical energy storage devices over the past 30 years. With the continuous explanation of application fields and regions, the high reliable and long-time operation of LIBs under subfreezing conditions plays an important role on promoting the economic and social development [1]. Especially, the average winter temperatures in northern China, which would be the main battlefield of economic development in the future, are consistently below 0 °C, as shown in Fig. 1a. Moreover, LIBs are also need to be applicated under several complex extreme subfreezing conditions, including manned aviation, deep-sea exploration, polar scientific research and space exploration [2]. Taking the electric vehicles (EVs) as an example, the global stock of EVs is projected to reach an astounding of 230 million units by 2030 according to estimation by the International Energy Agency. However, according to the penetration rate (PR) of EVs in various regions of China in 2023, the extension and application of EVs in cold area are dramatically restricted (Fig. 1b). Commercial LIBs still face significant performance degradation under low-temperature environments, including significant energy decay, poor charge ability, and short cycle life decline, which limit their adaptability and distribution. As for the typical Panasonic 18,650 Li ion cell, it can only deliver an extremely low power and energy density retention of 1.25 % and 5 % when the temperature drops from 25 °C to −40 °C [3]. Additionally, it has been reported before that the state of charge of the LIB would be reduced by only 23 % when operated under −15 °C. Even worse, prototype LIBs based on ethylene carbonate (EC) system are unable to work due to the solidification of electrolytes under 0 °C.

Commercial LIBs consist of anodes, electrolytes, and cathodes, each of which significantly contributes to performance degradation under subzero temperature conditions. The low-temperature performance of LIBs is adversely affected by many factors, including increased viscosity and reduced ionic conductivity of the electrolyte, increased impedance of electrode materials and the voltage polarization caused by sluggish electrochemical reaction kinetics at the electrode-electrolyte interface (EEI) [4–7]. As is illustrated in Fig. 1c, Li^+ ions primarily undergo the following steps during the charging process: (a) extraction of Li^+ ions

* Corresponding author.
E-mail address: msrenzonghu@scut.edu.cn (R. Hu).

https://doi.org/10.1016/j.revmat.2025.100012
Received 21 March 2025; Received in revised form 5 April 2025; Accepted 5 April 2025
Available online 7 April 2025

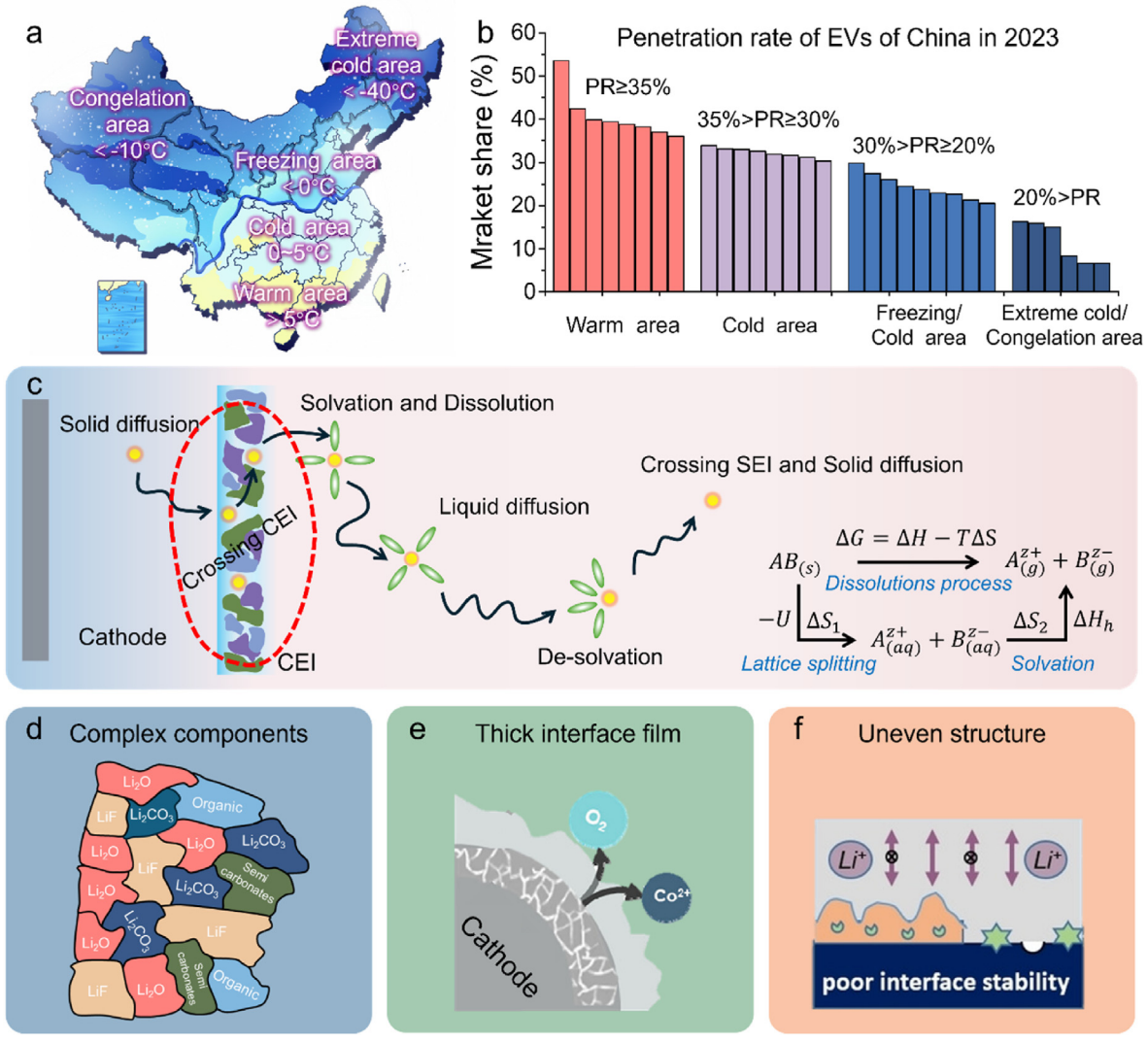

Fig. 1. Failure mechanism of low-temperature LIBs on the perspective of interfaces in the cathode materials. (a) Schematic diagram of winter temperature distribution in China along with the related (b) the penetration rate of EVs in 2023. (c) Interfacial migration diagram and kinetics issue of lithium ions during the discharging process, as well as several structural problems of CEI film, including (d) complex components, (e) thick interface film, and (f) inhomogeneous structure. Reported from Refs. [22,23] with permission, Copyright 2022–2023, Wiley-VCH, American Chemical Society.

from the cathode materials, (b) diffusion of the CEI film and solvation in the electrolyte, (c) migration of Li^+ ions through the electrolyte, (d) de-solvation from the electrolyte and crossing over the solid electrolyte interphase (SEI), and (e) insertion of Li^+ ions into the anode materials. The viscosity of electrolyte systems is crucial for stable operation of LIBs. Generally, electrolyte shows decreasing viscosity with temperature dropping, which contributes to the poor connection between the electrode and electrolyte, thus resulting in the large de-solvation/solvation energy [8–13]. As the critical step in the migration of Li^+ ions, de-solvation process is thought to have a significant effect on the impedance resistance. The dissolution process of various lithium salts can be divided into two distinct stages, including the dissociation of the lattice governed by lattice energy (U), and solvation with solvents determined by solvation energy (ΔH_h). Inserted formula in Fig. 1c lists the simplified Born-Haber formula for the dissolution process, where $\Delta H = -U + \Delta H_h$ and $\Delta S = \Delta S_1 + \Delta S_2$. According to this formula, a smaller Gibbs free energy (ΔG) indicates an easier dissolution process, and it can be indicated that the increased lattice energy of Li salt would result in reduced solubility, whereas an increase in solvation energy would cause increased solubility [14]. Such increased de-solvation energy seriously would hinder the insertion/extraction of Li^+ ions in the electrode, accompanied by the inhibition of Li^+ ions diffusion kinetics and a significantly augmented charge-transfer resistance (R_{ct}) [15–18]. Consequently, to extend to more application ranges, a number of substantial optimization methods have been proposed at the aim of reducing de-solvation energy and regulating interfacial kinetics.

As the main cost part of 30 % for the total cost in the battery production, cathode materials face the inevitable capacity constraint compared to those of the anode materials, which limits the further limitations of low-temperature LIBs [19]. Nowadays, researchers mainly focus on the crystal and structural designs of cathode materials to enhance their low-temperature electrochemical performance, including regulating microstructure and heteroatoms doping. Microstructural regulation mainly aims to increase the surface area of cathode materials with improved electronic conductivity, such as 0D nanoparticles, 1D nanowires and nanobelts, 2D nanoplates or nanosheets, as well as 3D complex nanostructures [20]. Heteroatom doping aims to expand the bulk interlayer spacing and then promotes internal Li^+ ion diffusion rates of cathode materials, including single atom doping, diatomic doping, and polyatomic doping. However, in addition to the cathode itself, the CEI film plays an important role on the diffusion pathway of Li^+ ions and electron transfer during the cycling process under low temperatures,

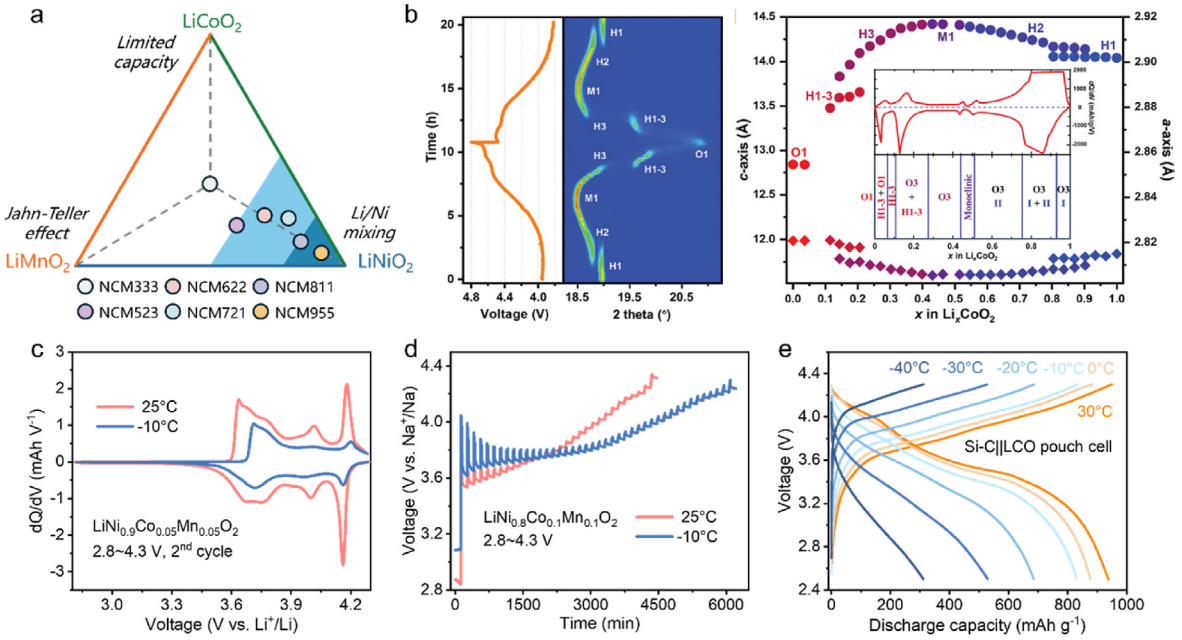

Fig. 2. Phase transition and electrochemical performance of layered oxide cathodes under cool environments. (a) Schematic diagram of the composition of layered oxide cathode materials. (b) In-situ PXRD evolution of (003) peak with corresponding charge-discharge profile of $LiCoO_2$ in the corresponding *dQ/dV* curves. Reported from Ref. [27] with permission. Copyright 2024, Wiley-VCH. (c) The 2nd *dQ/dV* curve of $LiNi_{0.9}Co_{0.05}Mn_{0.05}O_2$ cathode under 25 °C and −10 °C, (d) the GITT curve of $LiNi_{0.8}Co_{0.1}Mn_{0.1}O_2$ cathode under 25 °C and −10 °C, as well as (e) cycling performance of Si-C||LCO pouch cells over the wide temperature from −40 °C to 30 °C. Reported from Ref. [28] with permission, Copyright 2024, Elsevier.

considering that interfacial charge transfer resistance is the primary contributor to battery resistance [21]. Therefore, investigating the formation process and competition of CEI film accounts for an important method to solve the working problem of LIBs in cold environments, and modifying suitable CEI film on the cathode side becomes a hotpot in the field of low-temperature LIBs. Though several works have been denoted to study the low-temperature property of CEI film, the working mechanism and formation process of CEI film on the low-temperature performance of LIBs is still unclear due to its structural diversity and complexity. Until now, the effect of low temperatures on CEI film can be summarized to the three parts. It is found that the composition of CEI film would get more complex and the proportion of organic components would be significantly increased, which is not conducive to protecting the cathode materials (Fig. 1d). Meanwhile, CEI film shows a tendency of generating thick (Fig. 1e) and inhomogeneous (Fig. 1f) under subzero temperature, and the resistance of the CEI would rapidly increase when operated below −20 °C.

Electrolytes are the main factor of inducing the formation of CEI film and accelerating interfacial charge transfer of cathode materials, but few works systematically summarized the impact of electrolytes on the construction of CEI on the cathode surface at low temperatures. Herein, we aim to provide an inspiration of the electrolyte design on modifying the CEI film of cathode materials and thereby achieving excellent low-temperature performance. Firstly, we discuss the present interfacial issues and the formation mechanism of CEI films of layered oxide cathodes under low temperature environment. Secondly, the influence of various electrolyte components on the formation of the CEI film on the layered oxide cathodes at low temperatures are detailly investigated and compared. Thirdly, considering the structural and property specificity of CEI film, a summary of the principles and application status of various advanced characterization testing methods is put forward. Finally, based on the impact of different electrolyte modification strategies on the enhancement of low-temperature electrochemical performance, the future development of electrolyte design matched with layered cathode materials in low temperature LIBs is further presented.

2. Interfacial issue of layered oxide cathodes at subzero temperatures

2.1. Low-temperature lithiation/de-lithiation mechanism of layered oxide cathodes

Transition metal oxides $LiMO_2$ (M = Co, Ni, Mn) with a-$NaFeO_2$ layered structure in Fig. 2a have garnered widespread attention due to the high redox potential and Li^+ ions mobility, since layered $LiCoO_2$ (LCO) is firstly reported as a cathode material for LIBs in 1980 [24]. LCO shows a typical crystal structure composed of O ions in the cubic close-packed stacking occupying the 6*c* positions, while Li and Co ions are located at the 3*a* and 3*b* positions and arranged in layered structures along the (111) crystal plane, forming an -ABCABC- stacking sequence [25,26]. Similarly, a series of layer oxide cathodes owns the same crystal structure, except for different occupancies of transition metals (TMs). Layered oxide cathodes would undergo a series of phase transitions induced via the lithiation and de-lithiation processes. Fig. 2b shows the *in situ* powder X-ray diffraction (PXRD) patterns with the related differential capacity/voltage (*dQ/dV*) curves of typical LCO. When charged to 4.7 V, there are five phase transitions with six structures appearing in LCO, including O3, H1-3, O1 phases [27]. Generally, H1-3 and O1 phases show poor electrochemical irreversibility, commercial LCO is only discharged to 4.2 V with the de-lithiation degree of 0.5, along with the H1-H2-M1-H3 phase, which are all related to O3 phase. Therefore, the actual capacity of commercial LCO is limited to around 140 mAh g^{-1}. $LiNiO_2$ cathode suffers from severe Li/Ni mixing issue and $LiMnO_2$ faces the irreversible dissolution of Mn ions due to the disproportionation reaction of Mn^{3+}. Ternary layered oxides of $LiNi_xCo_yMn_{1-x-y}O_2$ (NCM) have been extensively used now in power batteries for electric vehicles due to their combination of the advantages of LCO, $LiNiO_2$ and $LiMnO_2$ accompanied by a reduction usage of toxic and expensive Co. According to the mass ratio of TM elements, NCM could be divided into NCM333, NCM523, NCM622, and NCM811, and the capacity of the NCM increases with the increase of Ni content. Ni-rich cathode with Ni content over 80 % can provide the specific capacity more than 200 mAh g^{-1}. However,

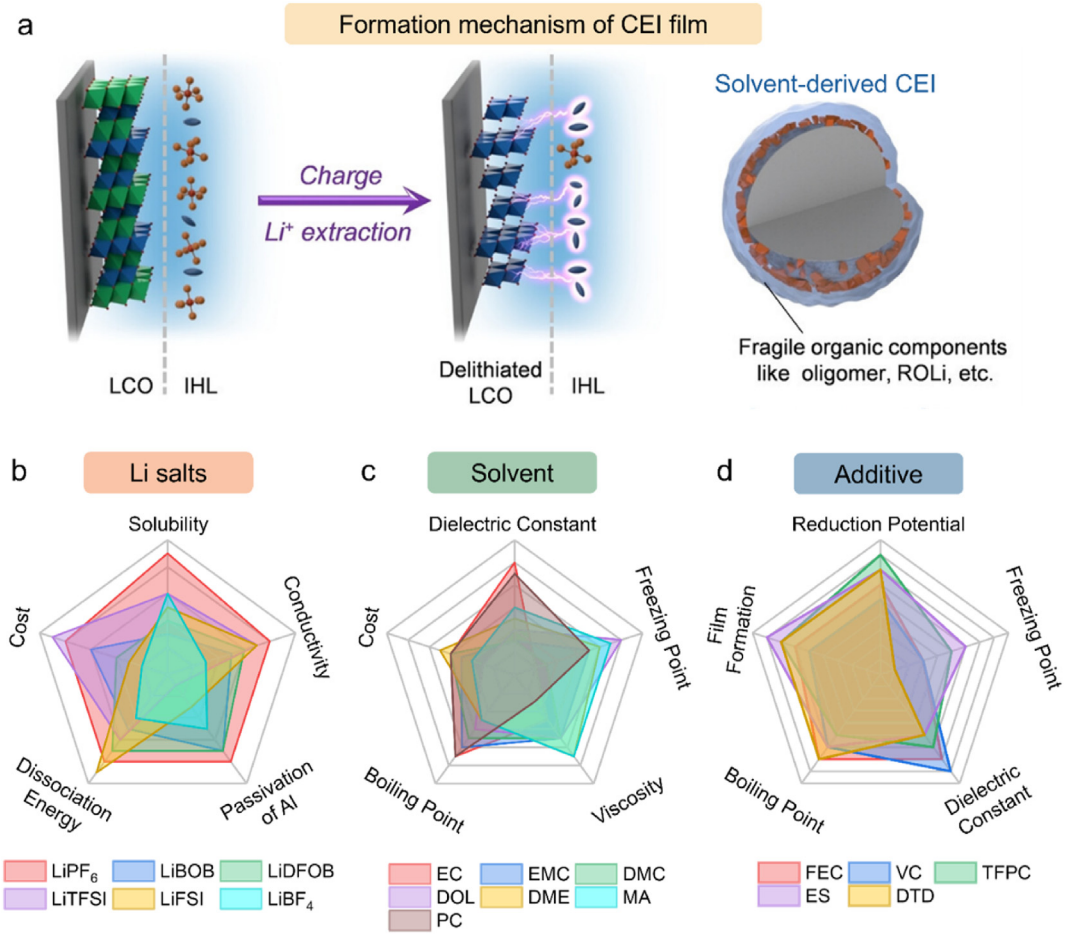

Fig. 3. Working mechanism of electrolyte system on the formation of CEI film on the layered oxide cathodes. (a) Schematic diagram of formation process of CEI layer on $LiCoO_2$ cathode via the electrolyte system. Reported from Ref. [29] with permission. Copyright 2022, Wiley-VCH. (b–d) The comparison of physical and chemical properties of (b) Li salts, (c) solvent, and (d) additives applied in low-temperature LIBs.

Ni-rich NCM materials still face some drawbacks, including interfacial high-impedance rock salt phases, residual LiOH and Li_2CO_3 layers, and the decomposition of electrolyte, which are particularly prominent at low temperatures.

The *dQ/dV* curve and GITT measurement are the two key tools for exploring the low-temperature electrochemical kinetics reaction of cathode materials, and Fig. 2c displays the 2nd *dQ/dV* profile of NCM955 cathode under 25 °C and −10 °C. As can be seen, the voltage plateau of the NCM955 cathode shows clear change under −10 °C, resulting in a clear shift in the position of the characteristic peak with a large electrochemical overpotential, indicating the weaken internal phase transition process and slow charge mass transfer of the cathode materials. In addition, NCM955 cathode shows the broaden characteristic peak under −10 °C, which may be due to the slow electrochemical reaction rate and poor discharge/charge ability. Fig. 2d shows the GITT curve for the NCM811 cathode during the initial charge-discharge process under 25 and -10 °C, and it is seen that severe capacity degradation and electrochemical polarization would occur with the temperature decreases. Operated under 25 °C, the oxidation process of $Ni^{2+/3+}$ and $Ni^{3+/4+}$ takes place preferentially over the oxidation process of $Co^{3+/4+}$, while Co can suppress the cation mixing of Li and Ni atoms. Mn^{4+} remains electrochemically inert and does not participate in the redox process, introducing Mn^{4+} can maintain the stability of the structure and reduce costs. When operated at subzero temperature, the initial discharge plateaus of the layered oxide cathode gradually rise, while the initial discharge capacity gradually declines. As for the full pouch cell, the effects of low-temperature condition on restricting the Li^+ ion diffusion during the cycling process are more prominent, and thereby lead to a reduction in the discharge capacity (Fig. 2e) [28].

2.2. Formation mechanism of CEI induced via electrolyte components

The formation mechanism of CEI film involves complex electrochemical reactions shown in Fig. 3a [29]. During the charging process, Li^+ ions are deintercalated from the cathode materials, causing interfacial chemical state transition, which then reacts with the electrolyte to form a CEI film. After continuous cycling, a thick CEI film would be formed and play a protective role in the cathode material. To optimize the component of low-temperature electrolytes, including altering the solvents and solutes, as well as adding functional additives, the formation process and organic/inorganic component of CEI film would be fundamentally adjusted, thus accelerating the electrochemical kinetics of the cathode materials under cool environment. Moreover, such modulation strategies can also be targeted to regulate the physicochemical properties of the electrolyte, such as decreasing its melting point and viscosity, as well as increasing its conductivity, thereby enhancing Li^+ ion migration within the electrolyte at low temperatures.

Li salts are critical components of electrolytes and play a vital role in the development of low-temperature batteries. Battery performance can be affected by types, concentration and reactivity of Li salts. The most widely used Li salt is lithium hexafluorophosphate ($LiPF_6$) due to its balanced properties such as high dissociation constant and conductivity. When operated under low temperature, the solubility of traditional $LiPF_6$ in organic solvents would increase, which results in decreasing ionic

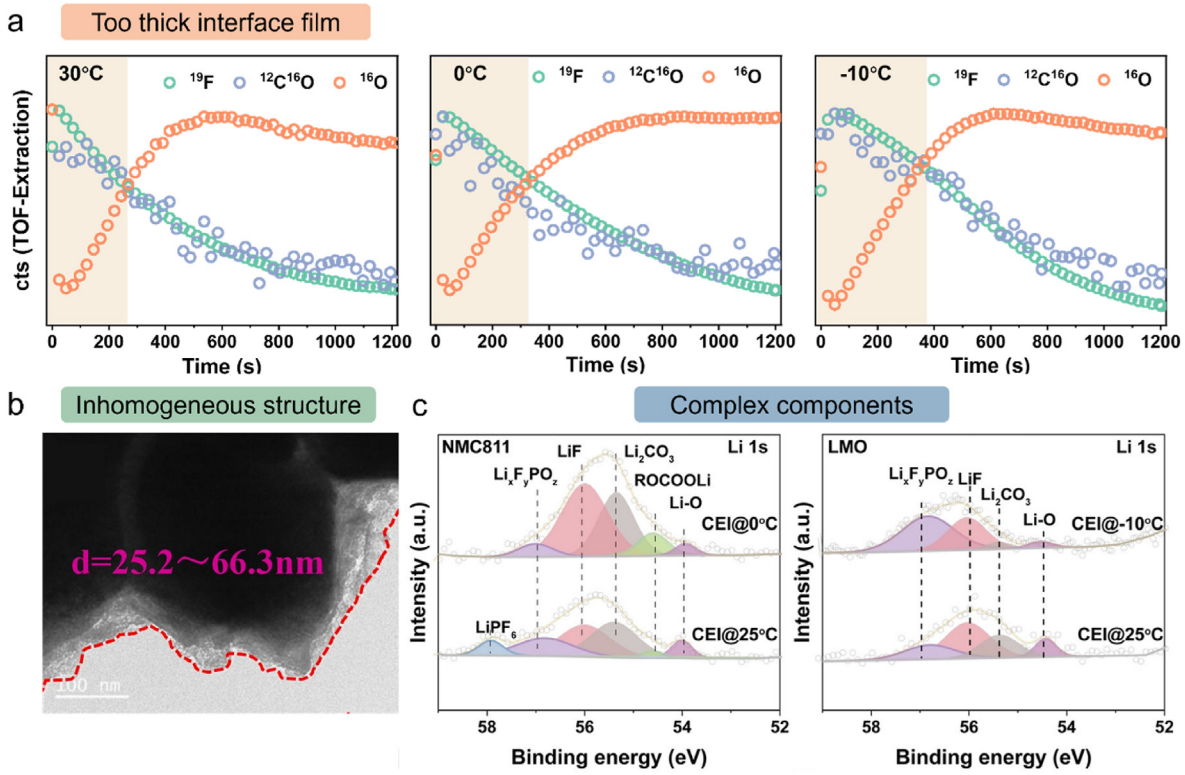

Fig. 4. Existed electrochemical kinetics and structural components of CEI film under cool environments. (a) Depth profile of ^{16}O, ^{19}F ions, and $^{12}C^{16}O$ cluster for the initial charged at 30 °C, 0 °C, and −10 °C. Reported from Ref. [32] with permission. Copyright 2024, Wiley-VCH. (b) TEM images of pristine NCM811 at −40 °C after cycling for 50 times. Reported from Ref. [33] with permission. Copyright 2021, Elsevier. (c) High-resolution XPS spectrum of cycled NCM811 and LMO cathodes at room and subzero temperatures. Reported from Ref. [34] with permission. Copyright 2024, American Chemical Society.

conductivity of the electrolyte system. Aimed Li salts should own high ionic conductivity and good solubility at low temperatures. Also, Li salts should possess better chemical and electrochemical stability without passivation of Al polar ear and decomposition during continuous cycling processes. Fig. 3b lists the low-temperature characteristics of commonly used lithium salts in LIBs. We can see that $LiPO_2F_2$, lithium difluoro(oxalato)borate (LiDFOB), lithium bis(trifluoromethanesulfonyl)imide (LiTFSI), and lithium bis(fluorosulfonyl)imide (LiFSI) are popular because of Li salts in developing low-temperature electrolyte. Solvent takes up almost 85 wt% of the whole electrolyte and its internal conductivity would straightly the Li^+ ion diffusion rate in the LIBs. Ethylene carbonate (EC) is chosen as the commercial primary solvent due to its high permittivity and excellent film-forming properties, and doped with dimethyl carbonate (DMC), diethyl carbonate (DEC) and ethyl methyl carbonate (EMC). However, high EC-based electrolyte would face significant decreased viscosity and even partly solidification below 0 °C due to its high melting point [19]. Thus, researchers tried to introduce cosolvent with low melting point and viscosity to improve the low-temperature properties. The most common strategies to optimize low-temperature electrolytes is designing the composition and ratio of electrolyte solvents by adding other sub-solvents to conventional carbonate electrolytes, including carbonates, carboxylates and other special organic solvents. As shown in Fig. 3c, boiling point, dielectric constant and price, besides the viscosity and freezing point, would also be the important factors in choosing and designing the composition of solvents. Propylene carbonate (PC), 1,3-dioxolane (DOL), and methyl acetate (MA) are commonly used solvents. In addition to these overall optimizations, incorporating certain additives introduced in formation of CEI films is another common approach. These functional electrolyte additives typically serve as three main purposes, i.e., assisting the formation of stable CEI film in electrolytes with poor film-forming capabilities, enhancing the ionic conductivity, reducing interfacial impedance of the CEI film, and inhibiting the formation of undesirable CEI film. Such additives with higher HOMO levels would be preferentially decomposed on the surface of the cathode and participate in the formation of the CEI film, which would prevent the decomposition of the electrolyte and alleviate the formation of the inactive rock-salt phase on the cathode materials, including FEC, VC, TFPC, ES, and DTD (Fig. 3d). Among them, fluorinated additives are a prevalent class of electrolyte additives, which can facilitate the formation of interfacial LiF-rich inorganic layer. Inorganic-rich layer can provide numerous grain boundaries to accelerate the migration of Li^+ ions. Consequently, interfaces rich in inorganic components are considered to have lower interfacial resistance and R_{ct}, better inhibiting electrolyte decomposition and offering superior low-temperature performance [30]. FEC is one of the most common fluorinated additives, and the electrode-electrolyte interfacial film it helps form, which is rich in LiF, is widely recognized for significantly improving the subzero-temperature capability and cycling stability of LIBs [31].

2.3. *Existing interfacial problem of CEI film at subzero temperatures*

As mentioned above, the formation of CEI film under low temperatures suffers from several issues, which are complex component, too thick and uneven structure. Firstly, CEI film in low-temperature batteries would become much thicker than that operated at room temperature during the initial discharge-charge process due to the different Li^+ ion diffusion rate between interface and bulk structure of the cathode materials. Then, caused by the restricted and inconsistent Li + ion diffusion path, the formation of CEI film exhibits the heterogeneous growing trends after continuous cycling. Moreover, even if the depth of discharge has been dramatically decreased, the chemical composition of interfacial CEI film on the cycled cathode remains complex and irregular.

Our group previously discussed the interfacial and internal phase

Table 1
Low temperature performance of LIBs with different electrolytes.

Film-forming mechanism	System	Lithium salt	Solvent	Additives	[Capacity/(mAh g^{-1}) or capacity retention]/(current density or C rate)/(temperature/°C)	Voltage range/V	References
Solvent	Li||NCM811	$LiPF_6$	MTFP/FEC		73.7 %/0.1C/-50 °C 66.2 %/0.1C/-60 °C	2.0–4.5	[36]
	Li||NCM811	$LiBF_4$	THF/TFPC		165.7 mAh g^{-1}/0.1C/-20 °C	2.7–4.3	[37]
	Li||LCO	LiDFOB	FEC/DMS/IF		88 %/(1/15) C/-70 °C	2.7–4.45	[38]
	Li||NCM811	LiFSI	AN/TTE		84.3 %/0.1C/-20 °C	2.8–4.4	[39]
	Gr||NCM811	LiFSI	EDFA	FEC	~75 %/0.2C/-30 °C ~60 %/0.2C/-40 °C	3.0–4.45	[40]
	Gr||NCM523	$LiPF_6$	EC/EMC/MA	FEC	51.4 %/0.2C/-20 °C	3.0–4.2	[41]
	Gr||NCM811	$LiPF_6$	MDFA/PFPN/FEC		~75.8 %/0.5C/-50 °C	2.7–4.3	[42]
	Gr||NCM811	LiFSI	EMC/TTE		~82 %/(1/3C)/-20 °C	2.6–4.3	[43]
	Gr||NCM811	LiFSI	FAN		109.7 mAh g^{-1}/0.1C/-80 °C	2.8–4.5	[44]
	Gr||NCM523	LiFSI	DiFEC/MTFC/HFME		~74.3 %/0.1C/-20 °C ~45.7 %/0.1C/-40 °C	3.0–4.2	[45]
Anions	Li||NCM523	$LiPO_2F_2$	LiDFP/G4/HFE	FEC	81.4 %/0.1C/-40 °C	2.8–4.3	[46]
	Li||NCM811	LiTFSI/$LiPF_6$/$LiNO_3$	THF/FEC		149.3 mAh g^{-1}/0.1C/-40 °C	2.7–4.2	[47]
	Gr||NCM811	LiFSI/LiTFSI/LiDFOB/$LiNO_3$/$LiPF_6$	EC/DMC		~99 %/0.1C/-20 °C	2.8–4.3	[48]
	Gr||LCO	LiFSI/LiDFOB	DMS		~80 %/2C/-20 °C ~86 %/0.1C/-50 °C	2.0–4.2	[49]
	Gr||NCM523	$LiPF_6$	GBL/FPPN	LiDFOB	125 mAh g^{-1}/0.1C/-20 °C 90 mAh g^{-1}/0.1C/-40 °C	2.5–4.2	[50]
Additives	Li||LCO	LiTFSI	MP/FEC/HFE	LiDFOB	76 %/0.3C/-70 °C	3.0–4.5	[51]
	Li||NCM523	LiDFOB	TMS/EA/FEC	HFE	75 %/0.1C/-40 °C	3.0–4.6	[52]
	Li||NCM90	$LiPF_6$/$LiNO_3$	EC/EMC/DEC	TPFPB	54.6 %/0.2C/-30 °C	3.0–4.5	[53]
	Li||NCM523	LiTFSI/LiTFPFB	PC/EC/EMC	$LiPO_2F_2$	~107 mAh g^{-1}/0.1C/-20 °C	2.7–4.3	[54]
	Li||NCM811	$LiPF_6$	DMC/EMC	BA/EC/$LiBF_4$	119.3 mAh g^{-1}/0.2C/-30 °C	2.75–4.2	[33]
	Li||NCM111	$LiPF_6$	EC/EMC/DEC	$LiPO_2F_2$	133 mAh g^{-1}/1C/-10 °C	3.0–4.4	[55]
	Gr||NCM523	$LiPF_6$	EC/EMC	EMI-BF_4	~58.6 %/0.5C/-20 °C	2.75–4.2	[56]
	Gr||NCM523	$LiPF_6$	EC/EMC	PFPMS	~66.3 %/0.5C/-20 °C	2.75–4.2	[57]
	Gr||NCM811	$LiPF_6$	EC/EMC/DEC	SPBS	~80.8 %/0.5C/-20 °C ~68.7 %/1C/-20 °C	2.75–4.2	[58]
	Gr||NCM111	$LiPF_6$	EC/PC/EMC	$CsPF_6$/TTMSPi/FEC	~75.8 %/1C/-18 °C ~40.7 %/1C/-40 °C	3.0–4.2	[59]
	Gr||NCM811	$LiPF_6$	EC/EMC/DEC	PMBS	~81.6 %/0.5C/-20 °C ~62.5 %/1C/-20 °C	2.75–4.2	[60]
Anions/Solvent	Li||NCM622	LiDFOB	ES		150 mAh g^{-1}/0.1C/-30 °C	2.8–4.5	[61]
	Li||NCM811	LiDFOB	GBL/EC/DEC		165 mAh g^{-1}/0.5C/0 °C 50 mAh g^{-1}/0.5C/-30 °C	2.7–4.3	[62]
	Li||NCM811	LiTFSI/LiDFOB	MP/EMC		~152 mAh g^{-1}/0.1C/-40 °C	2.5–4.3	[63]

evolution of Ni-rich cathodes at room and low temperatures [32]. *Ex situ* time-of-flight secondary ion mass spectrometry (TOF-SIMS) was carried out on the NCM811 cathodes at different charge states in the initial discharge process, and the results are shown in Fig. 4a. LiF and Li_2CO_3 are chosen as the main components to track the formation process of CEI film under 30, 0, and −10 °C. As can be seen, the initial generated CEI film shows clear thicker grow trends with the decrease in the tested temperature. This thick CEI film would impede diffusion of Li^+ ions, leading to incomplete phase evolution, and the large amounts of Li_2CO_3 would not only induce the increase of impedance but also consume more Li^+ ions, leading to poor discharge capacities. It is worth noting that the thickness of the CEI does not necessarily increase with decreasing temperature, and it is subject to different responses of different components of the electrolyte to temperature changes. To examine the uniformity and to reduce the thickness of the CEI layer to improve the low-temperature performance of the electrolyte, Lv et al. [33] designed a electrolyte used butyl acrylate (BA), EC and lithium tetrafluoroborate ($LiBF_4$) as mixed additives to optimize the solubility, conductivity and melting point. Fig. 4b displays the TEM image of the NCM811 cathode cycled under −40 °C for 50 cycles. It is observed that the CEI film of cycled NCM811 cathode is thick and uneven at low temperatures, due to a decrease in reaction kinetics, additives such as $LiBF_4$ have a higher film formation priority than EC, inducing a thinner and more homogeneous CEI [35]. For better investigating the component of CEI film of different layered cathodes under low temperatures, Zhang et al. [34] discussed the influence of fluorinated additives on the formation of CEI film on NCM811, LCO and LMO cathodes under 0, -5, and -10 °C. High-resolution X-ray Photoelectron Spectroscopy (XPS) spectrum in Fig. 4c indicates that the mass contents of LiF, Li_2CO_3, $Li_xPO_yF_z$ in CEI films under subzero temperatures show different change trends of different cathodes under low temperature, and the chemical component of CEI film are not clearly influenced via the depth of discharge of cathode materials and the decreased viscosity of electrolyte. Therefore, the differences in the reaction kinetic reduction of the different film-forming components at low temperatures should be taken into consideration when designing the electrolyte.

3. Low-temperature interfacial modifications on layered oxide via electrolyte modulation

Nowadays, there is an increasing improvement in low-temperature performance of electrolytes and a substantial disparity in low-temperature performance among different target electrolytes systems that utilize different Li salts, solvents, and additives, thus promoting the critical development of the thin, uniform, robust, and low impedance inorganic-rich CEI film. We summarize and compare various means of constructing CEI via electrolyte designing and compare the low-temperature performance achieved in different literature, aim to provide reference ideas and guidance for development of new low-

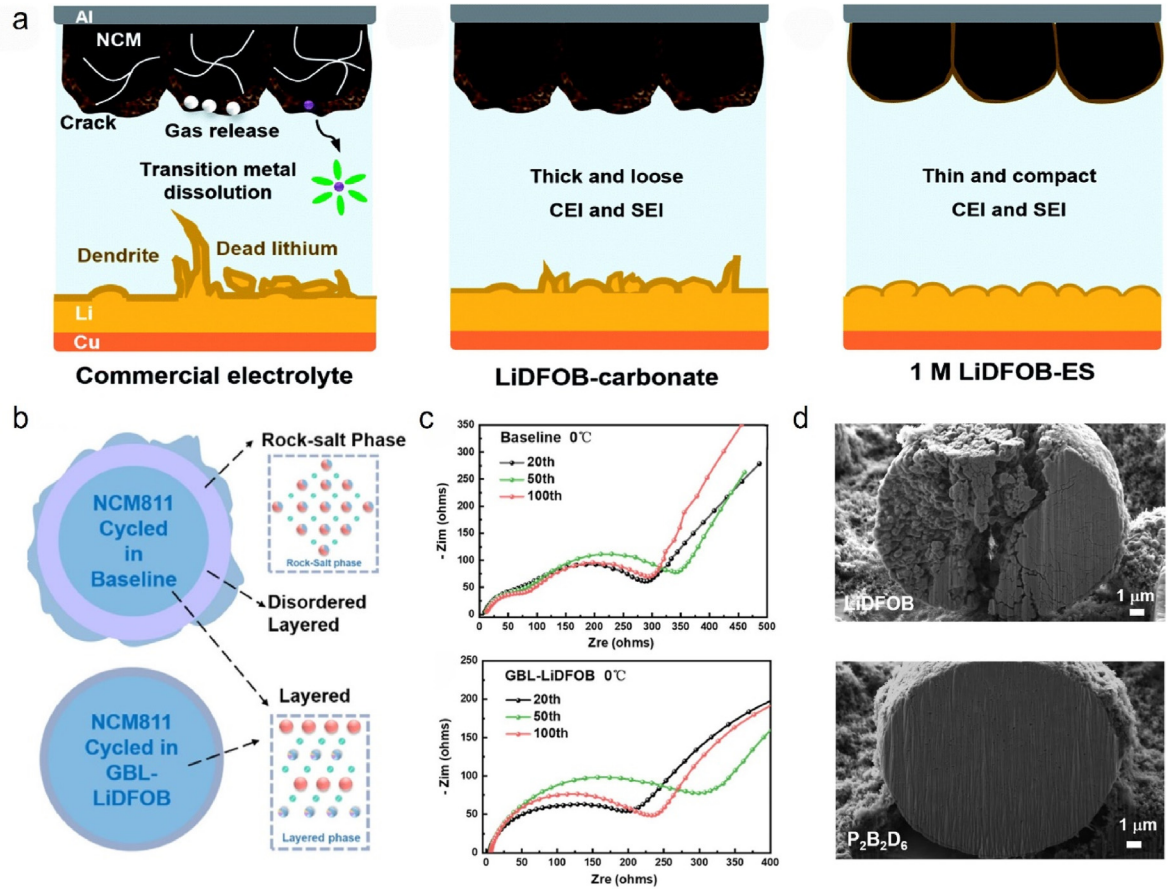

Fig. 5. Enhanced interfacial electrochemical kinetics via borates salt. (a) Schematic diagram of interface induced by various electrolytes. Reported from Ref. [61] with permission. Copyright 2022, The Royal Society of Chemistry. (b) Schematic diagram of interface modification. (c) Electrochemical impedance spectra with baseline and GBL-LiDFOB. Reported from Ref. [62] with permission. Copyright 2022, American Chemical Society. (d) Cross sectional SEM images of cycled NCM811 particles. Reported from Ref. [66] with permission. Copyright 2024, Wiley-VCH.

temperature electrolytes. Table 1 summarizes the low-temperature performance of different electrolytes based on different CEI film-forming mechanisms.

3.1. *Li slats*

Borates such as $LiBF_4$, lithium bis(oxalate)borate (LiBOB) and LiDFOB have attracted widespread attention from researchers due to their significant contribution to the improvement of the low temperature performance of LIBs. In 2002, $LiBF_4$ is found to own a higher low-temperature performance than that of $LiPF_6$, which can maintain more than 70 % discharge capacity of the RT under −40 °C because of the decrease of R_{ct} [64]. However, the SEI formed in $LiBF_4$ electrolyte is not sufficiently stable, which impairs the long-term cycle performance of the battery, and this is the reason why $LiBF_4$ has not been widely adopted in the battery community [33]. LiBOB possesses the advantage of inducing the formation of stable SEI under subzero temperature, but the poorer solubility and conductivity compared with $LiPF_6$ constrains its potential for broader application. Compared with LiBOB, LiDFOB inherits the SEI-inducing ability and has improved solubility and ionic dissociation characteristics [65], and is also used as an electrolyte additive widely.

Fang et al. [61] firstly designed an electrolyte with a simple formula of "single salt single solvent" enabling Li metal batteries (LMBs) to charge and discharge at −30 °C. The addition of LiDFOB into the carbonate solvents electrolyte represents an effective approach to alleviating certain issues to a certain extent. However, the problem of continuous consumption of LiDFOB persists. This leads to the thickening of the CEI, and consequently, significant degradation of battery performances at low temperatures. Thus, the researchers selected 1,2-ethylene sulfite (ES) as the only solvent, having close redox potentials to LiDFOB, facilitating the construction of an ultra-thin and robust CEI, thus contributing to a stable operation of low-temperature LMBs. Fig. 5a shows the challenges on interface when using commercial electrolyte, the function of the introduction of LiDFOB and the thin and compact CEI induced by the salt-solvent combination. With the 1M LiDFOB-ES electrolyte, the Li||NCM622 full-cells demonstrated a high reversible capacity of 150 mAh g^{-1}, and capacity retention rates were 88.4 % after 100 cycles under −30 °C, whereas the cell using the commercial electrolyte exhibited a capacity of only 20 mAh g^{-1}. Liang et al. [62] presented a low-temperature electrolyte in which γ-butyrolactone (GBL), possessing a low melting point and high ion conductivity, was utilized to partially substitute ethylene carbonate. This substitution could efficiently reduce the freezing point and enhance the ionic conductivity of the electrolyte at subzero temperatures. Simultaneously, as a cosolvent, GBL augments the dissolution of LiDFOB, facilitating the formation of an interfacial film rich in F-, B-, and O- at the Ni-rich cathode. Thereby, it suppresses the detrimental interface reaction and diminishes the interface impedance. Fig. 5b shows the schematic diagram of the induction of the CEI by GBL-LiDFOB, which can protect effectively suppressing the rock-salt phase caused by lithium-nickel mixing and protect the cathode from side reactions. From the TEM pictures of the cycled NCM811 cathode obtained at 0 °C, CEI derived from the baseline electrolyte is thick and uneven, comparatively, a thin and uniform interface film is covered on the surface when GBL-LiDFOB is employed, which would reduce the impedance and promoting Li^+ ions transfer at low temperatures. The EIS results in Fig. 5c show that the impedance of the cell used GBL-LiDFOB

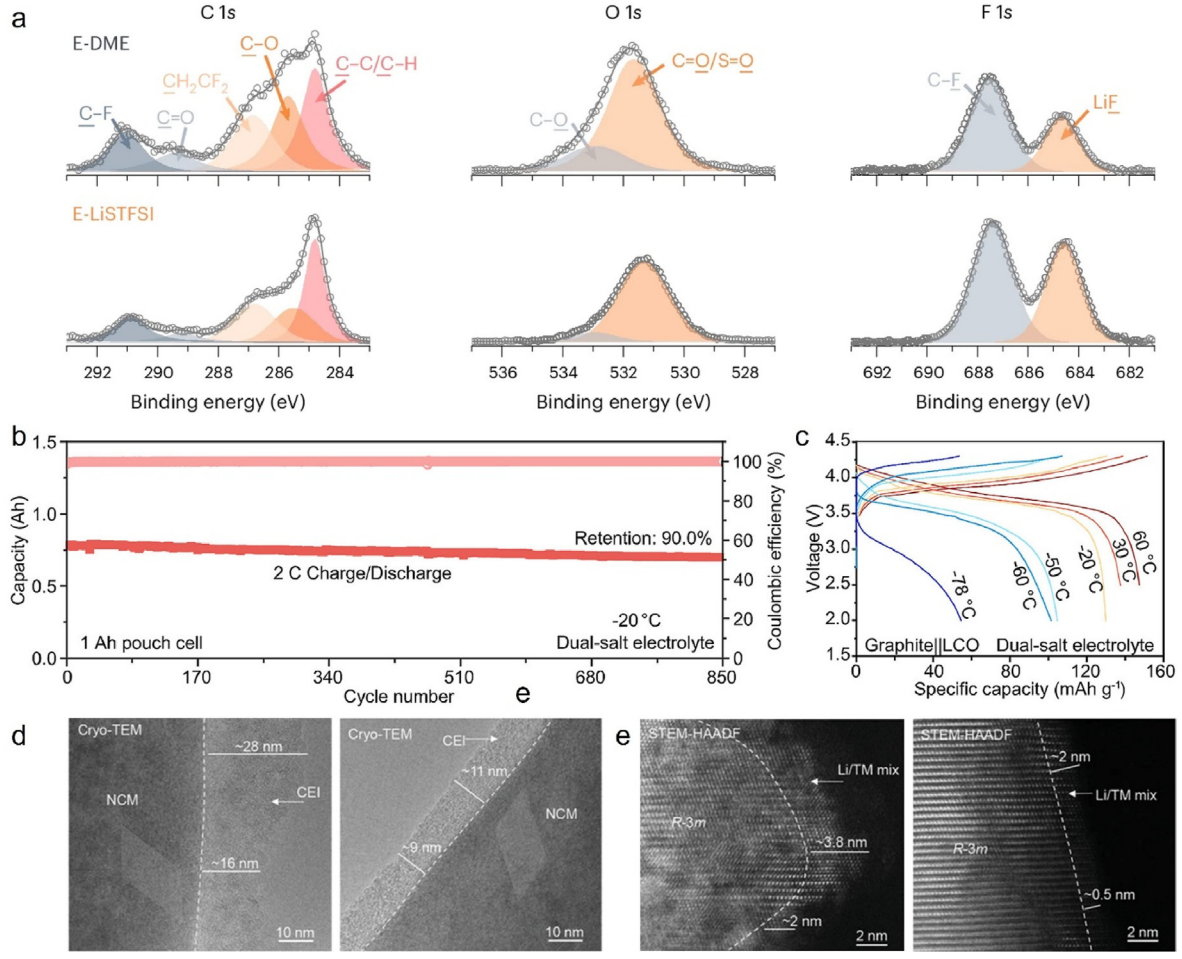

Fig. 6. Intact interfacial structural stability via sulfonamide systems. (a) XPS spectrum of the cycled NCM811 cathodes in different electrolytes after 30 cycles. Reported from Ref. [67] with permission. Copyright 2024, Springer. (b) Cycle performance of 1 A h pouch cell with LiFSI-LiDFOB-DMS electrolyte at 2C rate under −20 °C and (c) the voltage profiles under different temperatures. Reported from Ref. [49] with permission, Copyright 2023, American Chemical Society. (d) Cryo-TEM images of NCM811 cathode electrolyte interphase after cycling in different electrolytes. (e) Low-magnification STEM-HAADF images of NCM811 after cycling in different electrolytes. Reported from Ref. [48] with permission. Copyright 2024, Wiley-VCH.

after cycling is always lower than that of the cell using the baseline electrolyte. A non-concentrated and fluorine-free ether electrolyte was reported, dissolved ternary salts of LiDFOB, $LiPF_6$ and $LiBF_4$ in tetrahydrofuran (THF) [66]. Fig. 5d shows the SEM images of NCM811 cathode particles with this electrolyte that remained intact after 50 cycles, in contrast to the fragmented particles in the control group. Evident particle breakage can be observed for NCM811 particles in the control group in cross-sectional SEM images of cathode, which were collected using focused ion beam. It is also found that the significant proportion of inorganic constituents, such as $Li_xPO_yF_z$ and P-C components, would play a crucial role in enhancing the Li^+ conductivity within the CEI layer and concurrently contribute to the stabilization of Al foils.

Sulfonamide systems (LiTFSI and LiFSI) are also considered as other potential alternatives for $LiPF_6$ electrolytes below 0 °C by many researchers. These salts have advantages like preferentially decompose into a film on the electrode, high solubility and dissociation ability under subzero temperatures. Lin et al. [63] reported a low-temperature electrolyte with weak Li^+ coordination and low melting point, based on carboxylic ester methyl propionate (MP) with Li salts LiTFSI and LiDFOB. Characterization of the cycled NCM811 cathode by SEM and XPS reveals that the MP-based electrolytes tend to generate a thicker and LiF-rich CEI on surface of cathode than commercial electrolytes, which allows the manufactured Li||NCM811 cell to exhibit the superior long-term cycling stability. Lu et al. [67] designed and synthesized sulfoximide salts used in industrial pouch cells which worked under high rate and extreme low-temperature conditions named as lithium (trifluoromethanesulfinyl)(trifluoromethanesulfonyl)imide (LiSTFSI). By substituting sulfonyls with sulfinyls in LiTFSI, the salt was conferred distinctive oxidizability. A robust CEI with LiF dominated inner covered by negative-charged inorganic polymers enabled Li||NCM811 cells achieved 85.7 % capacity retention after 2000 cycles at −20 °C. The XPS analysis result in Fig. 5a shows that the organic components (O 1s signals) is gradually reduced and inorganic components (LiF signal in F 1s spectrum) are enriched in LiSTFSI-derived CEI and gradually increased with depth.

Also, dimethyl sulfite (DMS) is an effective low-temperature solvent [49], and the extensively dissociated LiFSI and DMS solvent can facilitate the swift conduction of Li^+ ions. Moreover, the strong affinity between $DFOB^-$ and Li^+ ions ensure the efficient desolvation of Li^+ ions across a broad temperature range. In the presence of electrolytes, an electric double layer (EDL) could rapidly form at the interface between the cathode and electrolyte, where the enriched species within the EDL preferentially decompose to build a sustainable CEI. The results of first-principle calculations show that LiDFOB consistently demonstrates the strongest interaction with LCO, irrespective of the charge state. This interaction facilitates the formation of an ultra-thin CEI, resulting in reduced interfacial impedance and exceptional low-temperature performance for the dual-salt electrolyte. The 1 Ah Graphite (Gr)||LCO pouch cell achieves 90 % capacity retention at 2C rate under −20 °C after 850 cycles (Fig. 6b), and it can even be charged and discharged at a rate of

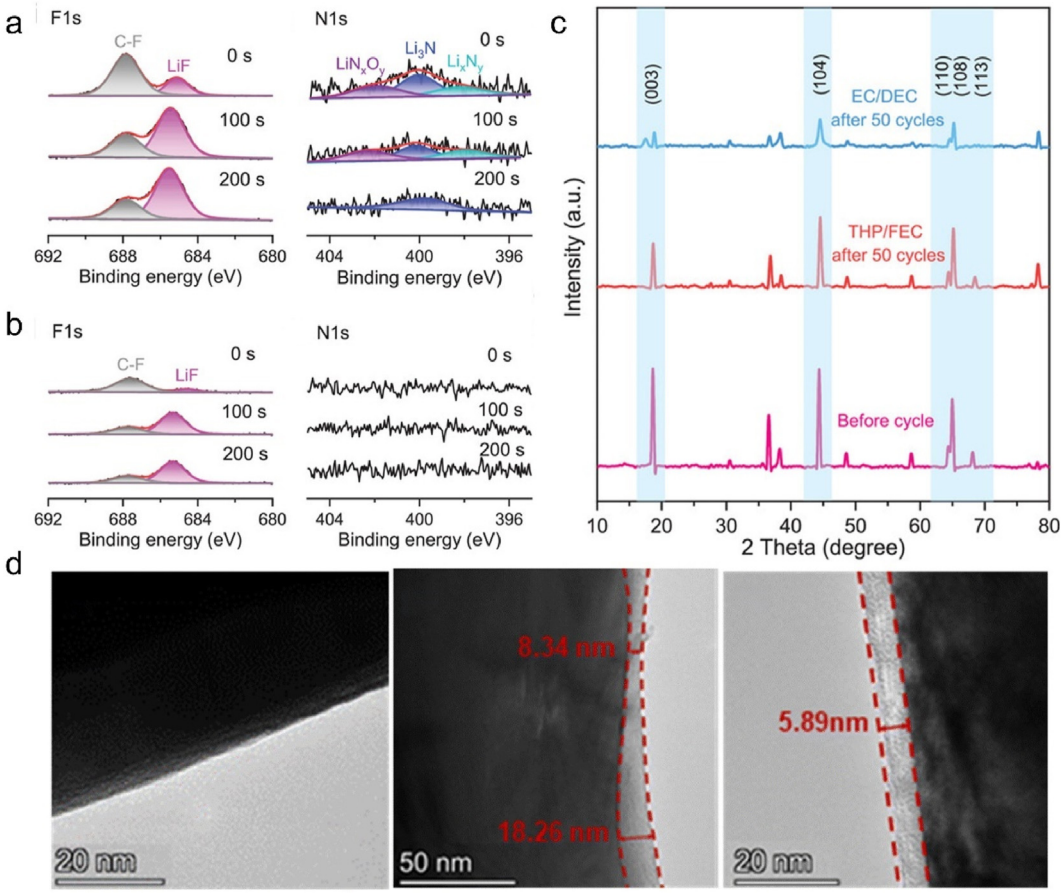

Fig. 7. Intact interfacial structural stability via solvent systems. (a, b) In-depth XPS spectra of NCM811 cathodes cycled under −20 °C in (a) THP/FEC electrolyte and (b) EC/DEC electrolyte. (c) XRD results of NCM811 cathodes before and after −20 °C cycling. Reported from Ref. [68] with permission. Copyright 2024, Wiley-VCH. (d) TEM images of pristine NCM811 cathode, NCM811 cathode cycled with standard electrolyte and NCM811 cathode cycled with LiFSI-AN-TTE. Reported from Ref. [39] with permission. Copyright 2024, The Royal Society of Chemistry.

0.01C at −78 °C (Fig. 6c). Liang et al. [47] developed an anti-freezing electrolyte with rapid kinetic achieved by a competitive coordination strategy based on the ternary-anion (TA) coupling of PF^{6-},$TFSI^{-}$, and NO^{3-} toward Li^{+}. The formulated TA electrolyte exhibits that low binding energy of Li^{+} anions, and high ionic conductivity, higher proportions of LiF and Li_3N in the constructed CEI are the reason why $TFSI^{-}$ and NO^{3-} decompositions are prior to, endowing the CEI with superior mechanical strength and low impedance. Additionally, the THF molecules would polymerize into the CEI layer, which could suppress further decomposition of electrolyte, while the CEI presents a homogeneous thickness of 2.5 nm. A high-entropy electrolyte with a unique solvation structure was reported to enhance the solubility of specific salts and stabilize electrode-electrolyte interfaces by incorporating multiple salts into the solution [48]. This high-entropy electrolyte was prepared by dissolving 1.0 M $LiPF_6$, 0.1 M LiFSI, 0.1 M LiDFOB, 0.1 M LiTFSI, 0.1 M $LiNO_3$ in EC/DMC (1:1 in volume) with 5 % fluoroethylene carbonate (FEC). Fig. 6d exhibits the cryo-TEM images of CEI layer of pristine materials and cathode cycled in high-entropy electrolyte. STEM-HAADF images reveal that the mixed Li/TM layer at the surface of NCM811 is thinner compared to that in commercial electrolyte (Fig. 6e). Moreover, the electron energy loss spectroscopy (EELS) confirms that the CEI is more stable due to its inorganic-rich species so that it could inhibit the expansion of cracks in the cathode materials. The Li||NCM811 cells demonstrated a high reversible capacity of 125 mAh g^{-1} at −40 °C, and capacity retention rates were 90 % after 60 cycles at 0.5C under −20 °C. Kuang et al. [46] introduced an LHCE electrolyte using $LiPO_2F_2$ as Li salt to achieve the anion-containing solvation structure with fewer solvent molecules. The $PO_2F_2^{-}$ can help form a uniform CEI rich in inorganic components (P-O, LiF) on the cathode interface which could effectively protect electrodes from parasitic reactions. The introduction of LiDFP effectively inhibits the dissolution of TM, thereby reducing the crosstalk phenomenon of the NCM523 cathode. Li||NCM523 cell exhibits enhanced discharge ability under subzero temperature with 81.4 % capacity at −40 °C and deliver 42.0 % capacity of RT at −60 °C. The selection of low-temperature Li salt should think over the types of cathodes, while standard and targeted selection and design principles should be established.

3.2. Solvents

In our previous work [18], we studied the low-temperature performance of plasma milling pretreated NCM622 cathode material sintered at 780 °C under two kinds of electrolytes, with EC/DEC and EC/PC/EMC solvent. The NCM622 cathode exhibits a higher discharge-charge capacity and better cyclic stability under the EC/PC/EMC electrolyte, both electrolytes remaining a stable mid-potential around 3.82 V for discharge at −10 °C and 0 °C, but when the temperature drops to −20 °C, severe polarizations occurred in the cathode under EC/DEC electrolyte, which results in initial discharge mid-potential dropping to 3.59 V with a very large voltage hysteresis of 0.71 V. In contrast, under EC/PC/EMC electrolyte the voltage hysteresis at −20 °C for the cathode is just 0.20 V, justified that the PC solvent can alleviate the degrees of low-temperature induced polarizations for the NCM622 cathode materials.

Li et al. [68] opted for tetrahydropyran (THP) as the principal solvent, FEC and $LiNO_3$ as the additives in the electrolyte design. This electrolyte formulation exhibits a reduced desolvation energy barrier and

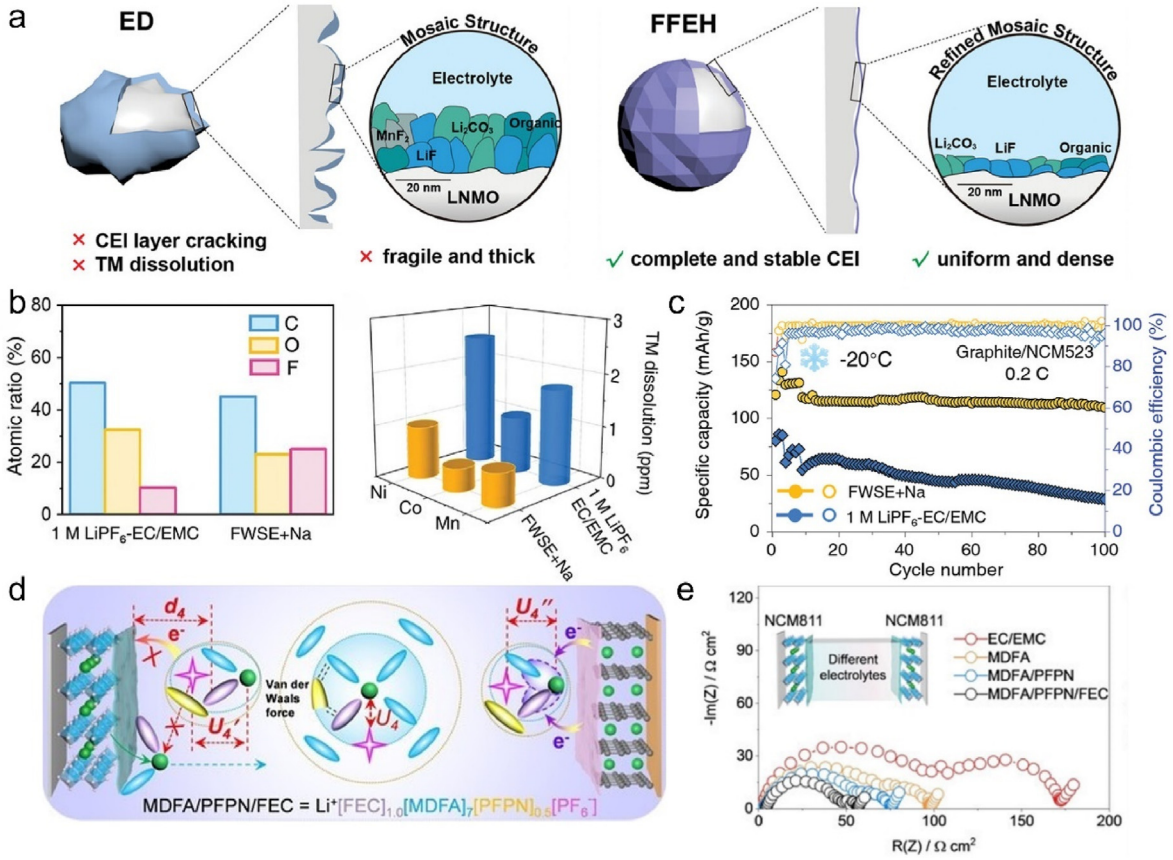

Fig. 8. Enhanced interfacial electrochemical kinetics reaction via solvent systems. (a) Schematic illustration of LNMO cathode configuration and CEI formation in different electrolytes. Reported from Ref. [71] with permission. Copyright 2024, Wiley-VCH. (b) Atomic ratios of C, O and F elements in the CEI and transition metal-dissolution analysis from cycled cathodes cycled in the two different electrolytes. (c) Long term cycling stability at −20 °C under 0.2C rate of NCM523-based full cells. Reported from Ref. [45] with permission. Copyright 2023, Wiley-VCH. (d) Graphic Li^+ solvation structure and interfacial model of MDFA/PFPN/FE. (e) EIS of the symmetric cell from the aged NCM811 electrodes. Reported from Ref. [42] with permission. Copyright 2022, Wiley-VCH.

demonstrates a relatively high ionic conductivity of 0.73 mS cm^{-1} even at an extremely low temperature of −50 °C. With the aid of TEM, a slender and homogeneous CEI film, possessing a thickness of 22 nm, could be discerned on the surface of the cathode based on the THP/FEC system. Through a comprehensive XPS analysis of the components within the CEI film, it was determined that the CEI film was constituted of LiF, Li_3N, and C-F compounds, all of which possess high ionic conductivity (Fig. 7a and b). These constituents are predominantly derived from the decomposition of FEC and NO_3^-. Their presence not only facilitates the accelerated transport of Li^+ within the CEI film at low temperatures but also stabilizes the cathode structure, effectively preventing phase transitions. Fig. 7c shows the X-ray diffraction (XRD) results of cathodes before and after cycling in various electrolytes. For the cathode cycled in EC/DEC, not only did it experience a weakening of the peak intensity of the characteristic crystal planes, which was the same as that of the cathode cycled in THP/FEC, but also the disappearance of the old peaks and the appearance of new peaks signified that severe structural damage had occurred to the cathode. Nitrile solvents such as acetonitrile (AN), nitrile butyronitrile (BN) and propionitrile (PN) exhibit lower melting points and viscosities than carbonate solvents. The strong interactions between cyanide and lithium ions endow nitrile solvents with strong solvation capabilities. Therefore, adding nitrile solvents to carbonate electrolytes effectively increases the electrolyte's low-temperature conductivity and enhances lithium ion migration kinetics [69]. However, the incompatibility of AN with anode and cathode materials has hindered its applications. A LHCE AN-based electrolyte comprising LiFSI and TTE diluent was developed by Liu et al. [39]. This AN-based electrolyte enables the formation of partially dissociated salt domains with high ratios of CIPs and AGGs [43,70]. With the assistance of the TTE diluent, the formation of the CEI rich in inorganic compounds be promoted, thereby facilitating enhanced Li^+ transport properties of the CEI under subzero temperatures. EIS results show that the CEI formed by the AN-based electrolyte exhibits relatively high impedance at RT but significantly lower impedance than the control electrolyte at −20 °C. TOF-SIMs results indicated that the inorganic components such as Li_2S and LiF concentrate on the inner layer of CEI while the outer layer is predominantly composed of organic components like $ROCO_2Li$ and PEO. TEM images exhibit a thinner and more uniform CEI layer induced by LiFSI-AN-TTE (Fig. 7d). This inorganic-rich inner layer effectively suppresses further electrolyte decomposition and CEI growth while facilitating improved Li^+ transport kinetics at the interphase under subzero temperatures.

Fan et al. [71] constructed a robust and thin CEI layer for $LiNi_{0.5}Mn_{1.5}O_4$ (LNMO) cathode, characterized by high ionic conductivity, to fulfill the requirements of low temperature conditions using a specially designed electrolyte 1 M $LiPF_6$ in FEC/3,3,3-fluoroethylmethyl carbonate (FEMC)/ethyl propionate (EP)/1,1,2,2-tetrafluoroethyl-2,2,2-trifluoroethyl ether (HFE). Fig. 8a shows the schematic of CEI on LNMO surface forming in designed electrolyte and control group. XPS reveals that the CEI is abundant in LiF and Li_2CO_3. The presence of Li_2CO_3 offers fast Li^+ transport kinetics, while LiF endows excellent electron-blocking capability, thereby reducing the ingress of electrons from LNMO into the CEI. This combination ensures the cycling stability of the battery, especially under low-temperature conditions. TOF-SIMs result indicated the presence of more organic fragments (C_2HO^-, $Li_2CO_3^-$) and inorganic fragments (PO_2^-) in the CEI layer of the LNMO surface, beneficial to prevent TM dissolution and to enhance rate and cycling performance.

Atomic force microscopy (AFM) result demonstrated Young's modulus of the CEI is approximately 415.8 MPa, nearly 20 times higher than the control group. Additionally, the CEI film in FFEH preserves the original spherical morphology of bulk LNMO, as evidenced by the relatively high roughness value and SEM images of the electrodes after cycling. Nan et al. [43] designed a low temperature electrolyte consisting of LiFSI, EMC and TTE diluent. EMC possesses a very small dipole moment (μ = 0.89D) indicating weaker ion-dipole interactions with Li^+, which suggests enhanced kinetics and reduced charge transfer resistance during the desolvation process [72]. When combined with the extrinsic assistance of TTE diluent, an anion-derived inorganic-rich CEI can be induced via the electrolyte, resulting in good stability and improved Li^+ transport properties for CEI. The Gr||NCM811 full cell with this electrolyte exhibits enhanced discharge ability under subzero temperature with the discharge capacity keeps 91 % of its RT at −20 °C. A LiF-rich CEI was induced by a fluorinated weakly solvating electrolyte (FWSE) consisting of 1 M LiFSI in trans-4,5-di-fluoroethylene carbonate (DiFEC)/methyl (2,2,2-trifluoroethyl) carbonate (MTFC)/hexafluoroisopropyl methyl ether (HFME) [45]. XPS results reveal that the ratio of F element in CEI induced by FWSE solvent was nearly twice the value of the comparison electrolyte. Inductively coupled plasma mass spectrometry (ICP-MS) tests confirm that fewer TMs (Ni, Co, Mn) dissolute from cathode with the use of FWSE (Fig. 8b). The formation of thin and high LiF content CEI was tightly correlated with the highly fluorinated FWSE, which endowed the Gr||NCM523 cell deliver a capacity retention of 92.1 % after 100 cycles, while the cell with $LiPF_6$-EC/EMC maintains a capacity of only 28.6 mAh g^{-1} (Fig. 8c).

Carboxylates represent another prevalent category of low-temperature electrolyte solvent, with lower melting points and viscosities than linear carbonates, which are perceived as more conducive for improving the low-temperature performance of electrolytes. A 1 M $LiPF_6$ in a methyl 3,3,3-trifluoropionate (MTFP)/FEC (9:1) electrolyte has been reported by Holoubek [36]. The author specifically mentioned that the Coulombic Efficiency (CE) for the first cycle is only 60 %, which is attributed to the formation of a robust CEI. Organic fluoride dominant CEI compositions can be observed on the surface of NCM811 cathode cycled in the MTFP-based electrolyte. The all-fluorinated electrolyte provided 161, 149, and 133 mAh g^{-1} when discharged at −40, −50, and −60 °C. Feng et al. [73] developed a methyl acetate (MA) based LHCE with a new short-chain fluorinated diluent named as 1,1,2,2-tetrafluoroethyl methyl ether (TFME). Compared with the LHCE used EMC as main solvent, the Li_2CO_3 accounted for more of the carbon compounds on the CEI film of MA-TFME electrolyte. It is found that denser and rich inorganic Li_xBF_y and LiF CEI can be formed on LNMO cathode surface, which would be more stable at high voltage and low temperature. The high content of LiF in the inorganic layer would reduce the impedance of CEI film, and then reduce the resistance of Li^+ shuttle in CEI film. The TFME-based LHCE demonstrated excellent stability with the LNMO cathode, and the battery could remain 80.85 % of its RT discharge capacity at 0.2C and −50 °C. Mo et al. [40] compared the low-temperature performance of the moderately fluorinated ethyl difluoroacetate (EDFA)-FEC electrolyte with ethyl acetate (EA), less-fluorinated ethyl fluoroacetate (EFA) and highly fluorinated ethyl trifluoroacetate (ETFA). EDFA exhibits lower binding energy than EFA and higher salt dissociation than ETFA, as confirmed by density functional theory (DFT). Nuclear magnetic resonance (NMR) spectra can further validate nearly all FSI^- anions stay as contact ion pairs (CIPs) and larger aggregates (AGGs), ultimately contributing to the formation of the CEI film formation. A thin and rich of LiF CEI layer can be observed on the surface of NCM811 cycled, which allowed the Gr||NCM811 full cell delivered discharge capacities of 141 and 113 mAh g^{-1} when the temperature declined to −30 and −40 °C. Zou et al. [42] designed a wide-temperature electrolyte with flame retardant by dissolving $LiPF_6$ in the mixed solvent of methyl difluoroacetate (MDFA), ethoxy-pentafluoro-cyclotriphosphazene (PFPN), and FEC. Fig. 8d shows the graphic Li^+ solvation structure and interfacial model of MDFA/PFPN/FEC electrolyte, Li^+ de-intercalated from the cathode which coordinates with free solvent could improving the anti-oxidation capability of solvent by the form of Li^+-solvent and enhancing the transfer rate of Li^+ ions. In contrast, Li^+ in EC/EMC electrolyte would preferentially interact with the free PF_6^- anion, which hinders the Li^+ transfer to the anode and intensifies the solvent dehydrogenation. The interfacial impedance of NCM811 cathode after 200 cycles in MDFA/PFPN/FEC was lowest among the four electrolytes compared (Fig. 8e). SEM and Fourier transform (FFT) images show no obvious microcracks in the cycled NCM811 cross section when using the MDFA/PFPN/FEC electrolyte. Although a few spinel-like phases appeared on the surface, the cycled NCM811 remained ordered and intact. In addition, the capacity retention of the full cell after 100 cycles was maintained at 87.4 % under 0.2C and 20 °C, and it delivered 75.8 % of the RT discharge capacity at 0.5C and −50 °C. Cui et al. [74] employed the molecular electrostatic potential (ESP) screening technique to single out 2,2-difluoroethyl trifluoromethanesulfonate (DTF) as cosolvent which displays a moderate minimum in molecular ESP, thereby achieving an equilibrium between excessively strong and excessively weak Li ions affinities. This property enables the sulfonyl group to efficiently attract Li ions without perturbing the solvation structure that is rich in anions.

Sulfate solvents such as dimethyl sulfite (DMS) and diethyl sulfite (DES) have exceptionally low melting points (<−110 °C) and viscosities (<0.9 cP), and the high dielectric constants of sulfate esters grant them great Li salt solvency and high ionic conductivity, making them promising candidates for low-temperature lithium battery electrolytes. Liu et al. [38] proposed a fluorine-sulfur electrolyte system based on LiDFOB, FEC, DMS and iso-butyl formate (IF) to achieve low solvation and high Li^+ saturation concentration (1.40×10^{-10} mol s^{-1}). XPS analysis of the CEI layers on various cathodes shows that the LiF content is highest in LCO (17.91 %), surpassing the contents in NCM811 (14.61 %), NCA (3.35 %), and LFP (0.21 %) cathodes. This high content is attributed to the strong binding energy and minimal lattice misfit between LiF and LCO. With the electrolyte, Li||LCO batteries deliver a discharge capacity of 110 mAh g^{-1} over 170 cycles under −70 °C. Zhang et al. [75] developed an electrolyte devoid of EC and characterized by weak solvation. This electrolyte was formulated by incorporating LiDFOB into a mixture of solvents, namely dimethyl sulfide (DMS), ethyl trifluoroacetate (ETFA), and fluoroethylene carbonate (FEC). The design objective was to make the reaction kinetics rise and to enhance the stability of the interfaces within low-temperature batteries. The CEI film was composed of LiF, B-F, SO_3F_x and Li_2S, this particular composition endows the film with both high ionic conductivity and elevated mechanical strength, thereby effectively preventing electrolyte corrosion and promoting the reaction kinetics.

3.3. Additive

Functional electrolyte additives can effectively introduce the formation of the stable and evenly CEI film with poor film-forming capabilities, thus resulting in enhanced ionic conductivity and reduced interfacial impedance. Inactive rock-salt phase on the cathode materials can be promoted via the addition of additives through the inhibition of the decomposition of the electrolyte. A B-rich CEI was induced by the $DFOB^-$ anion which decomposed prior to other components and adsorbed the surface of cathode [51]. Then, it is also found that $TFSI^-$ and B-containing species participated in the formation of CEI are also beneficial to the cathode during cycling, which can be attributed to the decomposition of HFE and further demonstrate the importance of LiDFOB. Moreover, FEC plays a crucial role in improving the antioxidation of the electrolyte and optimizing the composition of CEI film synergy with LiDFOB [52]. Furthermore, borate functional groups and high F concentration pentafluopropyl groups in TPFPB would preferentially adsorb on the Ni-rich cathode surface and inhibit the decomposition of carbonate-based electrolytes [53]. TPFPB not only participates in the construction of a B^- and F^- rich CEI with great Li^+ transport kinetics, but also helps improve the

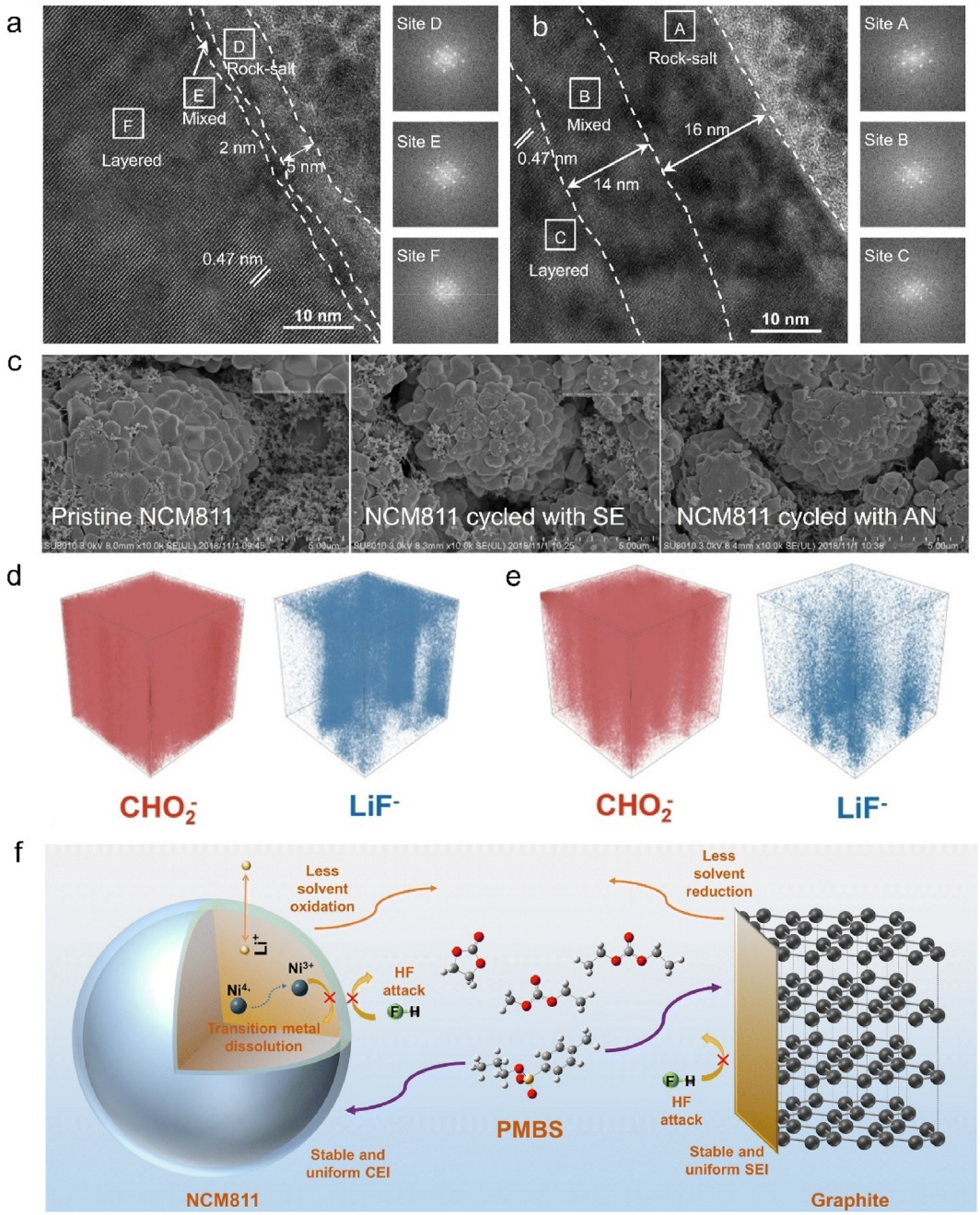

Fig. 9. Even interfacial structure with different species indueced via functional additives. (a, b) *Ex situ* TEM and fast Fourier transform (FFT) images of cycled NCM811 cathodes under basic electrolyte and with 1 %TPFPB after 100 cycles. Reported from Ref. [53] with permission. Copyright 2024, China Science Publishing & Media Ltd. (c) SEM images of pristine and cycled NCM523 cathode at −10 °C in the standard electrolyte and the electrolyte containing 1 % EMI-BF_4. Reported from Ref. [56] with permission. Copyright 2019, Elsevier. 3D rendering images for secondary fragments of CHO_2^- and LiF^- in CEI constructed by (d) EA/FEC/PS and (e) EA/FEC. Reported from Ref. [76] with permission. Copyright 2024, Wiley-VCH. (f) Schematic diagram of mechanism of action of the PMBS functional additive on the NCM811-based full cell. Reported from Ref. [60] with permission. Copyright 2024, The Royal Society of Chemistry.

solubility of $LiNO_3$, which is also beneficial to form an inorganic-rich SEI on Li metal anode. TEM images reveal that the introduction of TPFPB is beneficial to construct a thin rock-salt phase (5 nm) and mixed-phase (2 nm) on the surface of cathode (Fig. 9a), rather than that with basic electrolyte (Fig. 9b). Thus, manufactured Li||NCM811 cell exhibits a discharge capacity of 108 mAh g^{-1} at 0.2C under −30 °C with 1 % TPFPB in the based electrolyte.

$LiPO_2F_2$ could also be simply used as electrolyte additive to construct a low impedance CEI film and to enhance the electrochemical performance at low temperatures [55]. Wang et al. [56] introduced 1-ethyl-3--methylimidazolium tetrafluoroborate (EMI-BF_4) ionic liquid into $LiPF_6$-EC/EMC electrolyte as the low-temperature additive. Fig. 9c shows the SEM images of NCM523 disassembled from the cycled cell, a significant accumulation of electrolyte decomposition products was observed on the surface of the cathode, accompanied by the formation of cracks on certain particles. In contrast, the surfaces of the NCM523 particles remain smooth after 150 cycles in the electrolyte containing 1 % EMI-BF_4, while no noticeable organic decomposition products or cracks. The inclusion of EMI-BF_4 in the electrolyte promotes the formation of a stable CEI layer on the NCM523 cathode, thereby preventing continuous electrolyte decomposition and enhancing the structural stability of the cathode material. Also, 1,3-propanesultone (PS) was also chosen as the additive to

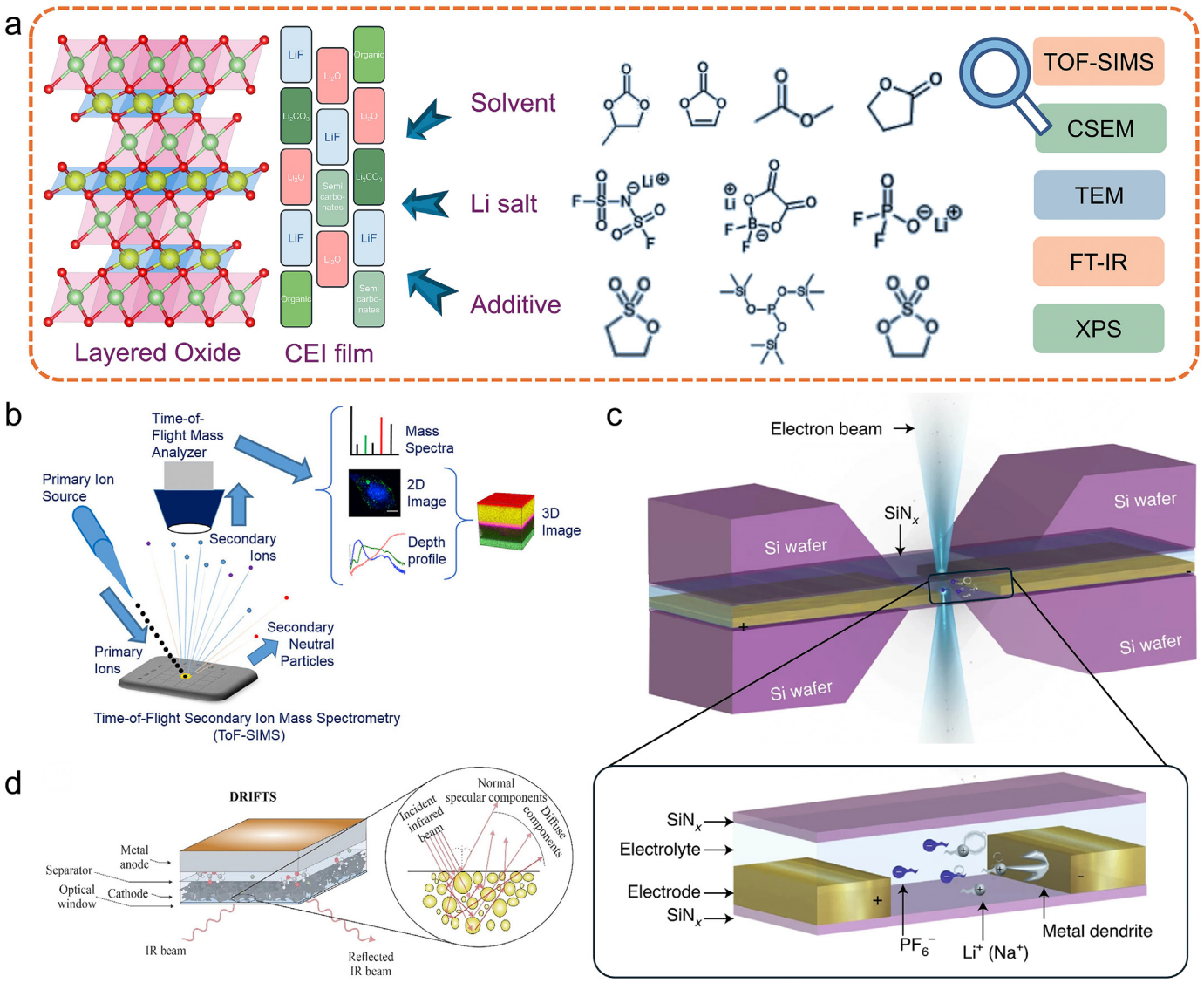

Fig. 10. Advanced equipment employed to detect the component and structure of CEI film. (a) Overview of typical advanced technique measurements. (b) Schematic diagram illustrating the fundamental principles of TOF-SIMS. Reported from Ref. [81] with permission. Copyright 2023, Frontiers in Chemistry. (c) Section view of electrochemistry liquid cell used in *in situ* TEM. Reported from Ref. [84] with permission. Copyright 2023, Springer Nature. (d) Schematic showing DRIFTS configuration used for *in situ* FTIR experiments. Reported from Ref. [86] with permission. Copyright 2023, Elsevier.

design the low-temperature electrolyte [76]. Theoretical computations jointly indicate that PS partakes in the formation of a resilient CEI comprising an inorganic inner layer and an organic outer layer. The inorganic constituents within this interface augment the stability of the interphase and establish pathways conducive to the transport of Li^+. Concurrently, sulfur-containing organic moieties enhance interfacial flexibility, thereby alleviating the accumulation of stress. Fig. 9d and e shows the 3D render images which analyze the chemical composition and spatial structure of CEI induced by EA/FEC/PS electrolyte (EAFP) and EA/FEC electrolyte (EAF). Within the CEI derived from EAFP, CHO_2^- fragments of feeble intensity aggregate on the CEI surface. Meanwhile, moderate LiF is present in the CEI derived from EAFP, which increases uniformly as the sputtering time prolongs and enriches within the inner layer of CEI. The Li||NCM811 cell using EAFP exhibits a capacity of 72 mAh g^{-1} after 200 cycles under −30 °C and can work in a wide temperature range. Shangguan et al. [54] developed a dual-salt electrolyte also used $LiPO_2F_2$ as additive. The cycle performance of dual-salt electrolyte with $LiPO_2F_2$ is much better than the electrolyte without $LiPO_2F_2$ under −20 °C, owe to the low impedance and protective CEI on NCM523 surface induced by $LiPO_2F_2$. Based on the MO theoretical calculation of the highest occupied molecular orbital (HOMO) energy, it can be deduced that the $LiPO_2F_2$ additive will undergo preferential oxidation. This suggests that the enrichment of Li_2CO_3, which contributes to ionic conductivity and P-O species on the surface of the NCM523 facilitated by $LiPO_2F_2$, is advantageous in preventing structural degradation and electrolyte oxidative decomposition. Consequently, this ensures the stable long-term operation of Li|| NCM523 cell under subzero temperatures.

Nowadays, many sulfone compounds have been used as electrolyte additives [77–79], and S-S bond and phenyl group were proved to have good influence on construction of EEI [80], including vinylene carbonate (VC) [57], and S-phenyl benzenethiosulfonate (SPBS) [58]. It is found that a certain additive combination in the electrolytes would create synergistic benefits on widening the working temperature of LIBs [59]. $CsPF_6$, FEC, 1,3-propane sultone (PS) and tris(trimethylsily) phosphite (TTMSPi) can be chosen as the additive combination to induce the formation of CEI film contains P-O-Si, F-enriched, or S-based, Cs-containing species and specifically numerous $Li_xPO_yF_z$. Li et al. [60] reported an additive which decomposes preferentially over solvent molecules named as propyl 4-methylbenzenesulfonate (PMBS). With 2 % PMBS in electrolyte, the NCM811 particles are intact with no cracks and the CEI layer

is thinner and more uniform than cathode used blank electrolyte. The capacity of the battery at −20 °C is 62.5 % of its capacity at RT under 1C. The schematic diagram of PMBS participating in the construction of CEI film is shown in Fig. 9f. Upon decomposition of the PMBS additive, a uniform and compact CEI film is generated on the cathode surface. This stable interfacial film serves dual functions: it shields the electrode interface from assaults by acidic substances like HF, and it simultaneously curbs the dissolution of TMs within the cathode as well as the decomposition of the electrolyte.

4. Advanced equipment on detecting the component and structure of CEI film

Advanced characterization techniques play a crucial role in research of CEI films, which assist researchers revealing the components and process of formation of CEI, as listed in Fig. 10a, typical advanced technique measurements include TOF-SIMS, CSEM, TEM, FT-IR and DEMS. TOF-SIMS is a highly sensitive technique that can both provide information of chemical composition and spatial distribution or sensitivity, which is particularly suited for surface and interface analysis and beneficial to battery research. Fig. 10b shows the schematics of the working principle of a TOF-SIMS, accelerated primary ions would bombard the sample surface, which leads to fragments of the species to get ionized. These are extracted and accelerated through electric fields into the TOF analyzer, which determines the mass-to-charge ratio (m/z) of each ion detected, and generated a two-dimensional image that provides information on element/molecule distribution with intensity on the sample surface [81]. In addition, TOF-SIMS enables the analysis of depth by applying dual-beam ion sources to etch the sample surface and analyzing the center of the sputtered crater. Through the combination of data derived from depth dependent mass spectrometry and 2D images, 3D imaging of sample composition can be accomplished, thereby furnishing information regarding sample morphology, structure, defects, and so on. Meng et al. [32] showed the growth of LiF layer in CEI at −10 °C and 30 °C with TOF-SIMS, revealing rapid LiF accumulation and accelerated CEI thickening at low temperatures.

For better observing the microstructure of the CEI film during the charge-discharge processes, a series of *in situ* electron microscope measurements are put forward. Liu et al. [82] investigated the electronic character change on the surface of cathodes during the formation of CEI in aqueous lithium-ion batteries via *in situ* scanning electrochemical microscopy (SEM). Changes in the average areal feedback current density (I_{avg}) correspond to changes in either increased substrate conductivity, the increased height of the substrate or these two in combination, which is influenced by the formation of CEI on cathodes surface. Zhang et al. [83] directly visualized the interface on the cathode via cryogenic electron microscopy. It was found that a conformal CEI layer *in situ* forming on cathodes with brief external electrical shorting, while an intimate CEI film does not exist at the single-particle level in commercial electrolyte under normal operation conditions. The common TEM can only be utilized for observing thin, stable and solid samples, and it has limitations in research of liquid samples that are not compatible with vacuum. *In situ* TEM encloses liquid samples by using a sufficiently thin and transparent silicon nitride (SiN_x) window that allows electrons to pass through the liquid layer, thereby providing opportunities for *in situ* studies of electrochemical reactions in the liquid phase. Fig. 10c presents the section view of the electrochemical liquid cell device for *in situ* TEM [84]. Magnified view of the electron beam irradiation area therein illustrates the electrochemical reactions to be observed, such as the formation of metal dendrites and the construction of CEI.

The principle of Fourier transform infrared (FTIR) spectroscopy is also used to emit light with continuous wavelengths, after infrared absorption by the sample, an interferogram is generated. Through Fourier transform, the interferogram is then converted into a spectrogram, so that the information about the chemical bonds (functional groups) of the sample can be obtained. Similar to Raman spectroscopy, it is also a vibrational technique, yet it has higher sensitivity. *In situ* FTIR spectroscopy serves as an effective tool for characterizing the EEI within electrochemical systems, because it has the ability to monitor the concentration variations of molecules/ions as well as charged or neutral adsorbed species on the material under the influence of the electrochemical potential [85]. Several configurations are typically used to minimize the absorption of IR radiation from the electrolyte species during *in situ* FTIR experiments, diffuse reflectance infrared Fourier transform spectroscopy (DRIFTS) is normally used for surfaces with poor reflectance. As shown in Fig. 10d, the beam interacts with a powder or a surface with high roughness and is reflected in all directions [86]. Kanamura et al. [87] used *in situ* FTIR to study the electrochemical oxidation of PC electrolyte on LCO thin film surface. It was demonstrated that the *in situ* FTIR could detect intermediates or products of electrochemical oxidation of non-aqueous electrolytes on cathode materials. The result shows that the electrochemical oxidation of propylene carbonate begins already at 4.1 V vs. Li/Li^+, PC is oxidized to $LiClO_4$ and some organic compounds have carboxylic groups. Cherkashinin et al. [88] found the evolution of core and valence band spectra related to the density of occupied and unoccupied states of CEI film on $Li_xNi_{0.2}Co_{0.7}Mn_{0.1}O_2$ by *in situ* synchrotron XPS. It has been shown that upon the deintercalation of Li^+ ions, the change in Fermi level could be observed, accompanied by oxidation of Ni^{2+} and Co^{3+} ions to compensate for the bulk charge. Hogrefe et al. [89] observed the growth of Li dendrites and internal short circuits directly in graphite||LFP and graphite||NCM 622 cells by using *in situ* optical microscopy set-up. The cross-sectional imaging data and electrochemical performance of batteries can be simultaneously recorded under various conditions, including progressively aggravated lithium metal deposition and the presence/absence of internal short circuits, which could potentially be employed to analyze the evolution of CEI under low-temperature conditions.

Despite the significant contributions of the aforementioned characterization techniques in elucidating the composition and formation mechanism of CEI, each analytical method still exhibits inherent limitations and drawbacks. Therefore, a judicious integration of complementary characterization approaches is imperative to compensate for their respective shortcomings. A typical example is TOF-SIMS, which suffers from several inherent limitations, including the inability to provide oxidation state information of detected species, differentiation of chemical species with similar associated fragmentation processes and material crystal structures, as well as constraints in lateral resolution and surface sensitivity [90]. *In situ* TEM characterization requires sufficiently thin and well-dispersed specimens to ensure adequate electron transparency and imaging resolution. However, such sample preparation requirements create testing conditions substantially different from actual battery operating environments, potentially compromising the representativeness of experimental results. *In situ* FTIR exhibits several inherent limitations, including: (1) micrometer-scale spatial resolution constrained by the fundamental diffraction limit of infrared wavelengths, (2) significant signal attenuation due to high reflectivity of metallic electrodes leading to reduced sensitivity in interfacial reaction detection, and (3) inevitable discrepancies between simulated *in situ* environments and realistic battery operating conditions. Therefore, when employing various advanced characterization techniques to investigate the formation and evolution of the CEI under low-temperature conditions, it is imperative to strategically integrate complementary characterization approaches by leveraging their respective strengths while compensating for individual limitations, thereby achieving the desired research objectives.

5. Conclusion and perspectives

In summary, this review focuses on the fundamental interfacial issues of layered cathode materials faced by low-temperature LIBs, including poor interfacial migration and kinetics issue of lithium ions and several structural problems of CEI film, including complex components, thick

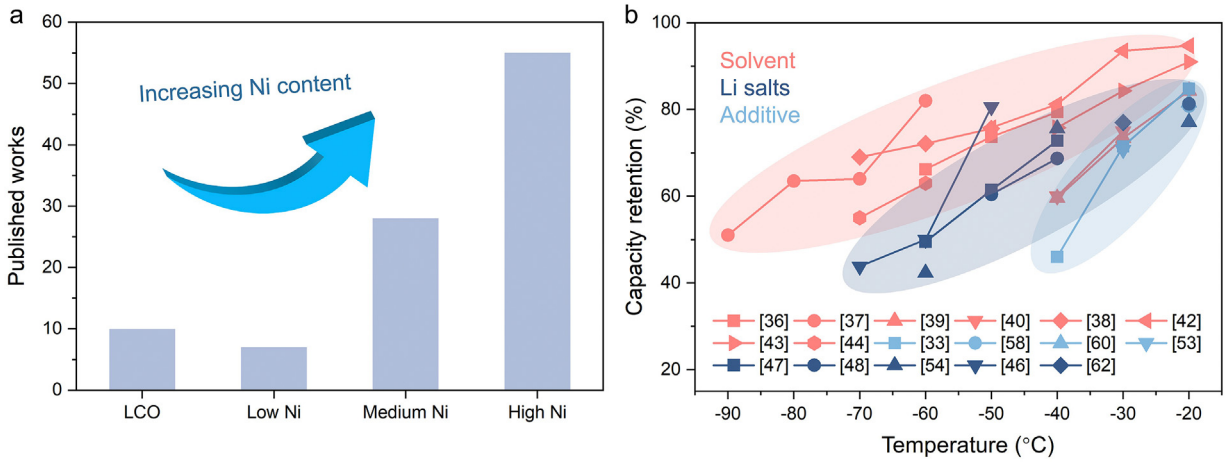

Fig. 11. Overview of existing literature about inducing CEI film via electrolyte modulation. (a) The number of recent published works based on the classification of $LiCoO_2$, low-Ni oxide, medium-Ni oxides, and high-Ni oxides, as well as corresponding (b) capacity retention of electrolyte system under freezing conditions.

interface film, and inhomogeneous structure. We study and discuss the various interfacial formation mechanisms of CEI induced via electrolyte components, i.e., Li slat, solvent and additives. Also, we summarize recent progress in the engineering of electrolyte inducing CEI construction and advanced characterization techniques on interface analysis.

For better understanding the relationship between Ni contents in the layered cathode with its low-temperature performance, we further summarize and classify the recent published works based on the layered oxide cathodes with different Ni content in Fig. 11a, i.e., LCO, low-Ni oxide (NCM111), medium-Ni oxides (NCM523 and NCM622), as well as high-Ni oxides (NCM811 and NCM9055), respectively. High-Ni oxides attract more attention of being applied in low-temperature LIBs, which may due to their high theoretical discharge capacity and electrochemical activity. It has been proved that higher Ni contents can effectively activate the phase transition and electrochemical redox under room and high temperatures, thus promoting the Li^+ ions diffusion rate and enhancing the discharge ability. However, the relationship between the Ni content and low-temperature electrochemical kinetics reaction is still unclear, which needs to be further investigated. Also, the high interfacial activity of high-Ni oxides would result in severe structural instability and inert $LiOH/Li_2CO_3$ layer, which restricts their daily storage and working life, and thus whether low-temperature storage could restrict this irreversible issue and promote the further commercial applications of Ni-rich oxides is also worth exploring. Moreover, study on the working state and mechanism of ultra-high Ni-rich oxide (more than 0.95) under low temperatures should also be further investigated.

Fig. 11b shows the capacity retention of cathode materials based on different electrolyte modulations under different temperatures, including targeted design of Li salts, solvent and additives. LiTFSI and LiFSI are the most popular Li salts for low-temperature applications in recent years because of their high ionic conductivity and good film forming properties, while LiDFOB is a desirable option to derive a LiF-rich, thin and robust CEI film on the cathode materials surface. As for additives, organic compounds with high F or B concentration groups may be a good choice to construct a F^- or B^- rich CEI with great Li^+ transport kinetics, S-S bond and phenyl group are also conducive to inducing a thin and protective CEI layer at low temperatures. Apparently, there are more studies on the design strategies of solvents and additives than those on Li salts. Besides the fact that the number of Li salts suitable for low-temperature environments is limited, another important reason is that the performance of low-temperature electrolytes achieved through solvent modification tends to be more excellent. It can be seen that these three modification methods show similar effects on the capacity retention above −20 °C, and then, these three modification methods exhibited significantly different regulatory abilities as the temperature further decreased.

Clearly, layered oxide cathode with strong CEI film induced by solvent molecules widely exhibited a higher capacity retention and wide temperature range down to even −90 °C. Adding functional additive shows the worst low-temperature performance and narrow working temperature of only −40 °C. The above discussion may apply a new sight that inducing CEI formation by changing the solvent composition might be a more effective method to enhance the performance of LIBs at subzero temperature. The terrible performance of LIBs under subzero temperature can be partially attributed to the uneven and thick CEI film on the surface of cathode. Given that the charge transfer process takes place at the interface between the electrode and electrolyte, the properties of this interface play a crucial role in the kinetics of charge transfer in LIBs. These interface properties have a profound impact on the low-temperature performance of LIBs, as they ultimately dictate the efficiency of charge transfer at lower temperatures. Among the modification strategies mentioned above, developing renewed solvent formulation is the most effective way to enhance the low-temperature performance. The solvation structure plays a prominent role in the transport of Li^+ ions in the electrolyte at low temperatures and largely determines the low temperature performance of the electrolyte. It is prevalent to design localized high concentration electrolytes and to achieve low de-solvation energy under subzero temperature, the use of fluorinated solvents contributes to the construction of inorganic-rich CEI.

CRediT authorship contribution statement

Zihan Xiong: Writing – original draft, Methodology, Investigation, Conceptualization. **Fanbo Meng:** Writing – original draft, Supervision, Conceptualization. **Jiahe Chen:** Resources, Methodology. **Zhenzhong Yang:** Resources, Methodology. **Renzong Hu:** Supervision, Project administration, Funding acquisition, Conceptualization. **Min Zhu:** Supervision, Project administration, Funding acquisition, Conceptualization.

Declaration of competing interest

The authors declare that they have no known competing financial interests or personal relationships that could have appeared to influence the work reported in this paper.

Acknowledgments

This work was supported by the National Natural Science Foundation of China (Nos. 52471227, 52231009 and 52404322), Guangdong Basic and Applied Basic Research Foundation (2023B1515040011), and the

Fundamental Research Funds for the Central Universities (2023ZYGXZR105). We also thank for the financial support from Open Research Fund Program of Hunan Mine Carbon Sequestration and Sink Enhancement Engineering Technology Research Center (No. 2024KSGTZH01).

References

[1] Z. Li, Y.-X. Yao, S. Sun, C.-B. Jin, N. Yao, C. Yan, Q. Zhang, 40 years of low-temperature electrolytes for rechargeable lithium batteries, Angew. Chem. Int. Ed. 62 (2023) e202303888, https://doi.org/10.1002/anie.202303888.

[2] D. Luo, M. Li, Y. Zheng, Q. Ma, R. Gao, Z. Zhang, H. Dou, G. Wen, L. Shui, A. Yu, X. Wang, Z. Chen, Electrolyte design for lithium metal anode-based batteries toward extreme temperature application, Adv. Sci. 8 (2021) 2101051, https://doi.org/10.1002/advs.202101051.

[3] G. Nagasubramanian, Electrical characteristics of 18650 Li-ion cells at low temperatures, J. Appl. Electrochem. 31 (2001) 99–104, https://doi.org/10.1023/A:1004113825283.

[4] J. Duan, J. Cui, H. Zheng, Aralia taibaiensis protects against I/R-induced brain cell injury through the Akt/SIRT1/FOXO3a pathway, Oxid Med Cell Long 2 (2019) 1, https://doi.org/10.1155/2019/7609765.

[5] H. Wu, X. Zhang, C. Wang, R. Cao, C. Yang, Experimental study on aerogel passive thermal control method for cylindrical lithium-ion batteries at low temperature, Appl. Therm. Eng. 169 (2020), https://doi.org/10.1016/j.applthermaleng.2020.114946.

[6] Y. Liu, Q. Duan, J. Xu, H. Li, J. Sun, Q. Wang, Experimental study on a novel safety strategy of lithium-ion battery integrating fire suppression and rapid cooling, J. Energy Storage 28 (2020) 101185, https://doi.org/10.1016/j.est.2019.101185.

[7] X. Wang, Y. Pan, X. Wang, Y. Guo, C. Ni, J. Wu, C. Hao, High performance hybrid supercapacitors assembled with multi-cavity nickel cobalt sulfide hollow microspheres as cathode and porous typha-derived carbon as anode, Ind. Crop. Prod. 189 (2022) 115863, https://doi.org/10.1016/j.indcrop.2022.115863.

[8] C. Yang, Y. Ren, B. Wu, F. Wu, Formulation of a new type of electrolytes for $LiNi_{1/3}Co_{1/3}Mn_{1/3}O_2$ cathodes working in an ultra-low temperature range, Adv. Mater. Res. 455–456 (2012) 258–264, https://doi.org/10.4028/www.scientific.net/AMR.455-456.258.

[9] R. Xiang, F.Q. Li, G.F. Jia, Z.J. Peng, Q. Zhuge, Effects of FEC additive on the low temperature performance of LiODFB-based lithium-ion batteries, Adv. Mater. Res. 724–725 (2013) 1025–1028, https://doi.org/10.4028/www.scientific.net/AMR.724-725.1025.

[10] Z.-M. Liu, D. Wang, S.-Z. Li, Q.-S. Lai, D.-R. Yang, L.-K. Zhao, J.-J. Mu, X.-C. Wang, X.-W. Gao, W.-B. Luo, An ultrafast rechargeable hybrid potassium dual-ion capacitor based on carbon quantum dot@ultrathin carbon film cathode, Rare Met. 43 (2024) 5070–5081, https://doi.org/10.1007/s12598-024-02719-4.

[11] J. Lin, Q. Zhou, Z. Liao, Y. Chen, Y. Liu, Q. Liu, X. Xiong, Steric hindrance engineering to modulate the closed pores formation of polymer-derived hard carbon for high-performance sodium-ion batteries, Angew. Chem. Int. Ed. 63 (2024) e202409906, https://doi.org/10.1002/anie.202409906.

[12] M. Su, Y. Chen, Y. Song, A. Dou, J. Wang, G. Yan, Y. Zhou, Z. Wang, Y. Liu, La_4NiLiO_8-assistant surface reconstruction to realize in-situ regeneration of the degraded nickel-rich cathodes, Chem. Eng. J. 477 (2023) 147202, https://doi.org/10.1016/j.cej.2023.147202.

[13] Z. Gong, Z. Liu, X.-W. Gao, N. Chen, Y. Song, X. Wu, A. Hu, Constructing cyclic hydrogen bonding to suppress side reactions and dendrite formation on zinc anodes, Chem. Eur J. 30 (2024) e202402558, https://doi.org/10.1002/chem.202402558.

[14] Z. Tian, Y. Zou, G. Liu, Y. Wang, J. Yin, J. Ming, H.N. Alshareef, Electrolyte solvation structure design for sodium ion batteries, Adv. Sci. 9 (2022) 2201207, https://doi.org/10.1002/advs.202201207.

[15] C.-B. Jin, N. Yao, Y. Xiao, J. Xie, Z. Li, X. Chen, B.-Q. Li, X.-Q. Zhang, J.-Q. Huang, Q. Zhang, Taming solvent-solute interaction accelerates interfacial kinetics in low-temperature lithium-metal batteries, Adv. Mater. 35 (2023) 2208340, https://doi.org/10.1002/adma.202208340.

[16] Z. Gao, Z. Lu, Y. Zhang, J. Xia, X. Zhang, C. Sun, Y. Yang, Y. Xu, K. Wang, X. Wang, J. Yao, Regulating interfacial desolvation via a weakly coordinating solvent molecule enhances Li-ion storage at subzero temperatures, Chem. Eng. Sci. 254 (2022) 117633, https://doi.org/10.1016/j.ces.2022.117633.

[17] S.Y. Vassiliev, V.V. Sentyurin, E.E. Levin, V.A. Nikitina, Diagnostics of lithium-ion intercalation rate-determining step: distinguishing between slow desolvation and slow charge transfer, Electrochim. Acta 302 (2019) 316–326, https://doi.org/10.1016/j.electacta.2019.02.043.

[18] C. Ji, Q. Zhou, Y. Yuan, W. Chen, T. Hou, B. Zhao, Y. Qin, X. Xiong, Electron-deficient sites on boron-doped graphite enable air-stable and durable red phosphorus anode for lithium-ion batteries, Energy Environ. Sci. 17 (2024) 4273–4282, https://doi.org/10.1039/D4EE00970C.

[19] A. Chakraborty, Service recovery in low contact context: an empirical study, Int. J. Indian Cult. Bus. Manag. 21 (2020) 262–278, https://doi.org/10.1504/ijicbm.2020.109744.

[20] Y. Ding, Z.P. Cano, A. Yu, J. Lu, Z. Chen, Automotive Li-ion batteries: current status and future perspectives, Electrochem. Energy Rev. 2 (2019) 1–28, https://doi.org/10.1007/s41918-018-0022-z.

[21] X. Ren, X. Zhang, Z. Shadike, L. Zou, H. Jia, X. Cao, M.H. Engelhard, B.E. Matthews, C. Wang, B.W. Arey, X.-Q. Yang, J. Liu, J.-G. Zhang, W. Xu, Designing advanced in situ electrode/electrolyte interphases for wide temperature operation of 4.5 V Li||$LiCoO_2$ batteries, Adv. Mater. 32 (2020) 2004898, https://doi.org/10.1002/adma.202004898.

[22] W. Dong, B. Ye, M. Cai, Y. Bai, M. Xie, X. Sun, Z. Lv, F. Huang, Superwettable high-voltage $LiCoO_2$ for low-temperature lithium ion batteries, ACS Energy Lett. 8 (2023) 881–888, https://doi.org/10.1021/acsenergylett.2c02434.

[23] H.-J. Guo, Y. Sun, Y. Zhao, G.-X. Liu, Y.-X. Song, J. Wan, K.-C. Jiang, Y.-G. Guo, X. Sun, R. Wen, Surface degradation of single-crystalline Ni-rich cathode and regulation mechanism by atomic layer deposition in solid-state lithium batteries, Angew. Chem. Int. Ed. 61 (2022) e202211626, https://doi.org/10.1002/anie.202211626.

[24] K. Mizushima, P.C. Jones, P.J. Wiseman, J.B. Goodenough, Li_xCoO_2 ($0<x<-1$): a new cathode material for batteries of high energy density, Mater. Res. Bull. 15 (1980) 783–789, https://doi.org/10.1016/0025-5408(80)90012-4.

[25] B.L. Ellis, K.T. Lee, L.F. Nazar, Positive electrode materials for Li-ion and Li-batteries, Chem. Mater. 22 (2010) 691–714, https://doi.org/10.1021/cm902696j.

[26] F. Meng, X. Xiong, L. Tan, B. Yuan, R. Hu, Strategies for improving electrochemical reaction kinetics of cathode materials for subzero-temperature Li-ion batteries: a review, Energy Storage Mater. 44 (2022) 390–407, https://doi.org/10.1016/j.ensm.2021.10.032.

[27] C. Lin, J. Li, Z.-W. Yin, W. Huang, Q. Zhao, Q. Weng, Q. Liu, J. Sun, G. Chen, F. Pan, Structural understanding for high-voltage stabilization of lithium cobalt oxide, Adv. Mater. 36 (2024) 2307404, https://doi.org/10.1002/adma.202307404.

[28] J. Chen, Y. Liu, F. Meng, S. He, J. Liu, Y. Zhao, K. Song, R. Hu, M. Zhu, Constructing ternary hybrid interface with rapid Li^+ conductivity to enable subzero-temperature Si-C||LCO pouch cell at -40 °C, Nano Energy 129 (2024) 110048, https://doi.org/10.1016/j.nanoen.2024.110048.

[29] J. Liu, J. Wang, Y. Ni, J. Liu, Y. Zhang, Y. Lu, Z. Yan, K. Zhang, Q. Zhao, F. Cheng, J. Chen, Tuning interphase chemistry to stabilize high-voltage $LiCoO_2$ cathode material via spinel coating, Angew. Chem. Int. Ed. 61 (2022) e202207000, https://doi.org/10.1002/anie.202207000.

[30] J.-P. Jones, M.C. Smart, F.C. Krause, R.V. Bugga, The effect of electrolyte additives upon lithium plating during low temperature charging of graphite-$LiNiCoAlO_2$ lithium-ion three electrode cells, J. Electrochem. Soc. 167 (2020) 020536, https://doi.org/10.1149/1945-7111/ab6bc2.

[31] A.C. Thenuwara, P.P. Shetty, N. Kondekar, S.E. Sandoval, K. Cavallaro, R. May, C.-T. Yang, L.E. Marbella, Y. Qi, M.T. McDowell, Efficient low-temperature cycling of lithium metal anodes by tailoring the solid-electrolyte interphase, ACS Energy Lett. 5 (2020) 2411–2420, https://doi.org/10.1021/acsenergylett.0c01209.

[32] F. Meng, H. Zhang, X. Xiong, X. Li, R. Wu, Q. Han, B. Qin, B. Yuan, R. Hu, Revealing the subzero-temperature electrochemical kinetics behaviors in Ni-rich cathode, Small 20 (2024) 2304806, https://doi.org/10.1002/smll.202304806.

[33] W. Lv, C. Zhu, J. Chen, C. Ou, Q. Zhang, S. Zhong, W. Lv, C. Zhu, J. Chen, C. Ou, Q. Zhang, S. Zhong, High performance of low-temperature electrolyte for lithium-ion batteries using mixed additives, Chem. Eng. J. 418 (2021) 129400, https://doi.org/10.1016/j.cej.2021.129400.

[34] L. Hong, Y. Zhang, P. Mei, B. Ai, Y. Zhang, C. Zhou, X. Bao, W. Zhang, Temperature-responsive formation cycling enabling LiF-rich cathode-electrolyte interphase, Angew. Chem. Int. Ed. 63 (2024) e202409069, https://doi.org/10.1002/anie.202409069.

[35] C.R. Yang, Y.Y. Wang, C.C. Wan, Composition analysis of the passive film on the carbon electrode of a lithium-ion battery with an EC-based electrolyte, J. Power Sources 72 (1998) 66–70, https://doi.org/10.1016/S0378-7753(97)02655-4.

[36] J. Holoubek, M. Yu, S. Yu, M. Li, Z. Wu, D. Xia, P. Bhaladhare, M.S. Gonzalez, T.A. Pascal, P. Liu, Z. Chen, An all-fluorinated ester electrolyte for stable high-voltage Li metal batteries capable of ultra-low-temperature operation, ACS Energy Lett. 5 (2020) 1438–1447, https://doi.org/10.1021/acsenergylett.0c00643.

[37] H. Hu, J. Li, Q. Zhang, G. Ding, J. Liu, Y. Dong, K. Zhao, M. Yu, H. Wang, F. Cheng, Non-concentrated electrolyte with weak anion coordination enables low Li-ion desolvation energy for low-temperature lithium batteries, Chem. Eng. J. 457 (2023) 141273, https://doi.org/10.1016/j.cej.2023.141273.

[38] J. Liu, B. Yuan, N. He, L. Dong, D. Chen, S. Zhong, Y. Ji, J. Han, C. Yang, Y. Liu, W. He, Reconstruction of LiF-rich interphases through an anti-freezing electrolyte for ultralow-temperature $LiCoO_2$ batteries, Engery Environ. Sci. 16 (2023) 1024–1034, https://doi.org/10.1039/D2EE02411J.

[39] L. Liu, Z. Shadike, X. Cai, M. Hong, Y. Gao, S. Shen, J. Zhang, Regulating the solvation structure of an acetonitrile-based electrolyte for Li/NMC811 batteries cycled at low temperature, J. Mater. Chem. A 12 (2024) 6947–6954, https://doi.org/10.1039/D3TA07347E.

[40] Y. Mo, G. Liu, Y. Yin, M. Tao, J. Chen, Y. Peng, Y. Wang, Y. Yang, C. Wang, X. Dong, Y. Xia, Fluorinated solvent molecule tuning enables fast-charging and low-temperature lithium-ion batteries, Adv. Energy Mater. 13 (2023) 2301285, https://doi.org/10.1002/aenm.202301285.

[41] N.D. Rodrigo, C. Jayawardana, B.L. Lucht, Investigation of the electrode-electrolyte interphase in ester-based electrolytes in NCM523/graphite cells, J. Electrochem. Soc. 169 (2022) 030519, https://doi.org/10.1149/1945-7111/ac5a19.

[42] Y. Zou, Z. Ma, G. Liu, Q. Li, D. Yin, X. Shi, Z. Cao, Z. Tian, H. Kim, Y. Guo, C. Sun, L. Cavallo, L. Wang, H.N. Alshareef, Y.-K. Sun, J. Ming, Non-flammable electrolyte enables high-voltage and wide-temperature lithium-ion batteries with fast charging, Angew. Chem. Int. Ed. 62 (2023) e202216189, https://doi.org/10.1002/anie.202216189.

[43] B. Nan, L. Chen, N.D. Rodrigo, O. Borodin, N. Piao, J. Xia, T. Pollard, S. Hou, J. Zhang, X. Ji, J. Xu, X. Zhang, L. Ma, X. He, S. Liu, H. Wan, E. Hu, W. Zhang, K. Xu, X.-Q. Yang, B. Lucht, C. Wang, Enhancing Li^+ transport in NMC811||graphite lithium-ion batteries at low temperatures by using low-polarity-solvent electrolytes, Angew. Chem. Int. Ed. 61 (2022) e202205967, https://doi.org/10.1002/anie.202205967.

[44] D. Lu, R. Li, M.M. Rahman, P. Yu, L. Lv, S. Yang, Y. Huang, C. Sun, S. Zhang, H. Zhang, J. Zhang, X. Xiao, T. Deng, L. Fan, L. Chen, J. Wang, E. Hu, C. Wang, X. Fan, Ligand-channel-enabled ultrafast Li-ion conduction, Nature 627 (2024) 101–107, https://doi.org/10.1038/s41586-024-07045-4.
[45] X. Zheng, Z. Cao, W. Luo, S. Weng, X. Zhang, D. Wang, Z. Zhu, H. Du, X. Wang, L. Qie, H. Zheng, Y. Huang, Solvation and interfacial engineering enable -40 °C operation of graphite/NCM batteries at energy density over 270 Wh kg^{-1}, Adv. Mater. 35 (2023) 2210115, https://doi.org/10.1002/adma.202210115.
[46] S. Kuang, H. Hua, P. Lai, J. Li, X. Deng, Y. Yang, J. Zhao, Anion-containing solvation structure reconfiguration enables wide-temperature electrolyte for high-energy-density lithium-metal batteries, ACS Appl. Mater. Interfaces 14 (2022) 19056–19066, https://doi.org/10.1021/acsami.2c02221.
[47] P. Liang, H. Hu, Y. Dong, Z. Wang, K. Liu, G. Ding, F. Cheng, Competitive coordination of ternary anions enabling fast Li-ion desolvation for low-temperature lithium metal batteries, Adv. Funct. Mater. 34 (2024) 2309858, https://doi.org/10.1002/adfm.202309858.
[48] Q. Wang, C. Zhao, Z. Yao, J. Wang, F. Wu, S.G.H. Kumar, S. Ganapathy, S. Eustace, X. Bai, B. Li, J. Lu, M. Wagemaker, Entropy-driven liquid electrolytes for lithium batteries, Adv. Mater. 35 (2023) 2210677, https://doi.org/10.1002/adma.202210677.
[49] Y. Zhao, Z. Hu, Z. Zhao, X. Chen, S. Zhang, J. Gao, J. Luo, Strong solvent and dual lithium salts enable fast-charging lithium-ion batteries operating from -78 to 60 °C, J. Am. Chem. Soc. 145 (2023) 22184–22193, https://doi.org/10.1021/jacs.3c08313.
[50] Y. Gu, S. Fang, L. Yang, S.-i. Hirano, A non-flammable electrolyte for long-life lithium ion batteries operating over a wide-temperature range, J. Mater. Chem. A 9 (2021) 15363–15372, https://doi.org/10.1039/D1TA01088C.
[51] P. Lai, B. Huang, X. Deng, J. Li, H. Hua, P. Zhang, J. Zhao, A localized high concentration carboxylic ester-based electrolyte for high-voltage and low temperature lithium batteries, Chem. Eng. J. 461 (2023) 141904, https://doi.org/10.1016/j.cej.2023.141904.
[52] S. Lin, H. Hua, P. Lai, J. Zhao, A multifunctional dual-salt localized high-concentration electrolyte for fast dynamic high-voltage lithium battery in wide temperature range, Adv. Energy Mater. 11 (2021) 2101775, https://doi.org/10.1002/aenm.202101775.
[53] D. Zhang, J. Ma, C. Zhang, M. Liu, K. Yang, Y. Li, X. Cheng, Z. Wang, H. Wang, W. Lv, Y.-B. He, F. Kang, A novel cathode interphase formation methodology by preferential adsorption of a borate-based electrolyte additive, Natl. Sci. Rev. 11 (2024) 219, https://doi.org/10.1093/nsr/nwae219.
[54] X. Shangguan, G. Xu, Z. Cui, Q. Wang, X. Du, K. Chen, S. Huang, G. Jia, F. Li, X. Wang, D. Lu, S. Dong, G. Cui, Additive-assisted novel dual-salt electrolyte addresses wide temperature operation of lithium-metal batteries, Small 15 (2019) 1900269, https://doi.org/10.1002/smll.201900269.
[55] J. Chen, L. Xing, X. Yang, X. Liu, T. Li, W. Li, Outstanding electrochemical performance of high-voltage $LiNi_{1/3}Co_{1/3}Mn_{1/3}O_2$ cathode achieved by application of $LiPO_2F_2$ electrolyte additive, Electrochim. Acta 290 (2018) 568–576, https://doi.org/10.1016/j.electacta.2018.09.077.
[56] W. Wang, T. Yang, S. Li, W. Fan, X. Zhao, C. Fan, L. Yu, S. Zhou, X. Zuo, R. Zeng, J. Nan, 1-ethyl-3-methylimidazolium tetrafluoroborate (EMI-BF_4) as an ionic liquid-type electrolyte additive to enhance the low-temperature performance of $LiNi_{0.5}Co_{0.2}Mn_{0.3}O_2$/graphite batteries, Electrochim. Acta 317 (2019) 146–154, https://doi.org/10.1016/j.electacta.2019.05.027.
[57] T. Yang, W. Fan, C. Wang, Q. Lei, Z. Ma, L. Yu, X. Zuo, J. Nan, 2,3,4,5,6-pentafluorophenyl methanesulfonate as a versatile electrolyte additive matches $LiNi_{0.5}Co_{0.2}Mn_{0.3}O_2$/graphite batteries working in a wide-temperature range, ACS Appl. Mater. Interfaces 10 (2018) 31735–31744, https://doi.org/10.1021/acsami.8b04743.
[58] H. Li, X. Zeng, X. He, W. Wang, W. Fan, C. Fan, Z. Ma, J. Nan, A S-phenyl Benzenethiosulfonate (SPBS)-containing electrolyte enhances the temperature performance of $LiNi_{0.8}Co_{0.1}Mn_{0.1}O_2$/graphite batteries by regulating the electrode interfaces, J. Power Sources 580 (2023) 233441, https://doi.org/10.1016/j.jpowsour.2023.233441.
[59] B. Liu, Q. Li, M.H. Engelhard, Y. He, X. Zhang, D. Mei, C. Wang, J.-G. Zhang, W. Xu, Constructing robust electrode/electrolyte interphases to enable wide temperature applications of lithium-ion batteries, ACS Appl. Mater. Interfaces 11 (2019) 21496–21505, https://doi.org/10.1021/acsami.9b03821.
[60] H. Li, J. Cai, J. Liao, Y. Li, X. Zeng, X. He, W. Fan, C. Fan, Z. Ma, J. Nan, A functional electrolyte containing propyl 4-methylbenzene sulfonate (PMBS) additive to improve the cycling performance of the $LiNi_{0.8}Co_{0.1}Mn_{0.1}O_2$/graphite full cell under the low temperature of -10 °C, J. Mater. Chem. A 11 (2023) 24970–24981, https://doi.org/10.1039/D3TA04535H.
[61] M. Fang, J. Chen, B. Chen, J. Wang, Salt-solvent synchro-constructed robust electrolyte-electrode interphase for high-voltage lithium metal batteries, J. Mater. Chem. A 10 (2022) 19903–19913, https://doi.org/10.1039/D2TA02267B.
[62] B. Liang, F. Cheng, X. Ge, X. Tan, C. Fang, J. Han, Tailoring electrolytes to enable low-temperature cycling of Ni-rich NCM cathode materials for Li-ion batteries, ACS Appl. Energy Mater. 5 (2022) 5867–5874, https://doi.org/10.1021/acsaem.2c00205.
[63] W. Lin, J. Li, J. Wang, K. Gu, H. Li, Z. Xu, K. Wang, F. Wang, M. Zhu, Y. Fan, H. Wang, G. Tao, N. Liu, M. Ding, S. Chen, J. Wu, Y. Tang, Weak-coordination electrolyte enabling fast Li^+ transport in lithium metal batteries at ultra-low temperature, Small 19 (2023) 2207093, https://doi.org/10.1002/smll.202207093.
[64] S.S. Zhang, K. Xu, T.R. Jow, A new approach toward improved low temperature performance of Li-ion battery, Electrochem. Commun. 4 (2002) 928–932, https://doi.org/10.1016/S1388-2481(02)00490-3.
[65] M. Genovese, A.J. Louli, R. Weber, C. Martin, T. Taskovic, J.R. Dahn, Hot formation for improved low temperature cycling of anode-free lithium metal batteries, J. Electrochem. Soc. 166 (2019) A3342, https://doi.org/10.1149/2.0661914jes.
[66] P. Liang, J. Li, Y. Dong, Z. Wang, G. Ding, K. Liu, L. Xue, F. Cheng, Modulating interfacial solvation via ion dipole interactions for low-temperature and high-voltage lithium batteries, Angew. Chem. Int. Ed. 64 (2025) e202415853, https://doi.org/10.1002/anie.202415853.
[67] Y. Lu, Q. Cao, W. Zhang, T. Zeng, Y. Ou, S. Yan, H. Liu, X. Song, H. Zhou, W. Hou, P. Zhou, N. Hu, Q. Feng, Y. Li, K. Liu, Breaking the molecular symmetricity of sulfonimide anions for high-performance lithium metal batteries under extreme cycling conditions, Nat. Energy (2024), https://doi.org/10.1038/s41560-024-01679-4.
[68] Z. Li, Y. Liao, H. Ji, X. Lin, Y. Wei, S. Hao, X. Hu, L. Yuan, Z. Huang, Y. Huang, A tetrahydropyran-based weakly solvating electrolyte for low-temperature and high-voltage lithium metal batteries, Adv. Energy Mater. (2024) 2404120, https://doi.org/10.1002/aenm.202404120.
[69] M.C. Smart, B.V. Ratnakumar, V.S. Ryan-Mowrey, S. Surampudi, G.K.S. Prakash, J. Hu, I. Cheung, Improved performance of lithium-ion cells with the use of fluorinated carbonate-based electrolytes, J. Power Sources 119–121 (2003) 359–367, https://doi.org/10.1016/S0378-7753(03)00266-0.
[70] J. Yang, X. Shi, W. Wang, Z. Liu, C. Shen, Localized high-concentration electrolyte (LHCE) for fast charging lithium-ion batteries, Batteries 9 (2023) 155, https://doi.org/10.3390/batteries9030155.
[71] X.-Y. Fan, M. Liu, T.-L. Chen, W. Hao, Z. Cao, N. Jiang, Q. Liu, Y.-H. Feng, H. Qin, S.-F. Chen, S. Liu, X. Ji, Y. Xiao, S. Chou, P.-F. Wang, Reconstructing inorganic-rich interphases by nonflammable electrolytes for high-voltage and low-temperature $LiNi_{0.5}Mn_{1.5}O_4$ cathodes, Adv. Funct. Mater. 34 (2024) 2400996, https://doi.org/10.1002/adfm.202400996.
[72] Y. Yang, Y. Yin, D.M. Davies, M. Zhang, M. Mayer, Y. Zhang, E.S. Sablina, S. Wang, J.Z. Lee, O. Borodin, C.S. Rustomji, Y.S. Meng, Liquefied gas electrolytes for wide-temperature lithium metal batteries, Energy Environ. Sci. 13 (2020) 2209–2219, https://doi.org/10.1039/D0EE01446J.
[73] T. Feng, G. Yang, S. Zhang, Z. Xu, H. Zhou, M. Wu, Low-temperature and high-voltage lithium-ion battery enabled by localized high-concentration carboxylate electrolytes, Chem. Eng. J. 433 (2022) 134138, https://doi.org/10.1016/j.cej.2021.134138.
[74] Z. Cui, D. Wang, J. Guo, Q. Nian, D. Ruan, J. Fan, J. Ma, L. Li, Q. Dong, X. Luo, Z. Wang, X. Ou, R. Cao, S. Jiao, X. Ren, Push-pull electrolyte design strategy enables high-voltage low-temperature lithium metal batteries, J. Am. Chem. Soc. 146 (2024) 27644–27654, https://doi.org/10.1021/jacs.4c09027.
[75] H. Zhang, X. Wu, W. Kong, M. Huang, Y. Xue, H. Xiang, Z. Huang, Tailoring electrolyte solvation of dimethyl sulfite with fluoride dominant via electrolyte engineering for enabling low-temperature batteries, Energy Storage Mater. 74 (2025) 103955, https://doi.org/10.1016/j.ensm.2024.103955.
[76] Y. Li, B. Wen, N. Li, Y. Zhao, Y. Chen, X. Yin, X. Da, Y. Ouyang, X. Li, P. Kong, S. Ding, K. Xi, G. Gao, Electrolyte engineering to construct robust interphase with high ionic conductivity for wide temperature range lithium metal batteries, Angew. Chem. Int. Ed. 64 (2025) e202414636, https://doi.org/10.1002/anie.202414636.
[77] G. Lan, L. Xing, D. Bedrov, J. Chen, R. Guo, Y. Che, Z. Li, H. Zhou, W. Li, Enhanced cyclic stability of Ni-rich lithium ion battery with electrolyte film-forming additive, J. Alloys Compd. 821 (2020) 153236, https://doi.org/10.1016/j.jallcom.2019.153236.
[78] X. Zheng, T. Huang, Y. Pan, W. Wang, G. Fang, M. Wu, High-voltage performance of $LiNi_{1/3}Co_{1/3}Mn_{1/3}O_2$/graphite batteries with di(methylsulfonyl) methane as a new sulfone-based electrolyte additive, J. Power Sources 293 (2015) 196–202, https://doi.org/10.1016/j.jpowsour.2015.05.061.
[79] R. Wang, X. Dai, Z. Qian, Y. Sun, S. Fan, K. Xiong, H. Zhang, F. Wu, In situ surface protection for enhancing stability and performance of $LiNi_{0.5}Mn_{0.3}Co_{0.2}O_2$ at 4.8 V: the Working Mechanisms, ACS Mater. Lett. 2 (2020) 280–290, https://doi.org/10.1021/acsmaterialslett.9b00476.
[80] M. Zhao, X. Zuo, X. Ma, X. Xiao, L. Yu, J. Nan, Diphenyl disulfide as a new bifunctional film-forming additive for high-voltage $LiCoO_2$/graphite battery charged to 4.4 V, J. Power Sources 323 (2016) 29–36, https://doi.org/10.1016/j.jpowsour.2016.05.052.
[81] F. Jia, X. Zhao, Y. Zhao, Advancements in ToF-SIMS imaging for life sciences, Front. Chem. 11 (2023) 1237408, https://doi.org/10.3389/fchem.2023.1237408.
[82] S. Liu, D. Liu, S. Wang, X. Cai, K. Qian, F. Kang, B. Li, Understanding the cathode electrolyte interface formation in aqueous electrolyte by scanning electrochemical microscopy, J. Mater. Chem. A 7 (2019) 12993–12996, https://doi.org/10.1039/C9TA03199E.
[83] Z. Zhang, J. Yang, W. Huang, H. Wang, W. Zhou, Y. Li, Y. Li, J. Xu, W. Huang, W. Chiu, Y. Cui, Cathode-electrolyte interphase in lithium batteries revealed by cryogenic electron microscopy, Matter 4 (2021) 302–312, https://doi.org/10.1016/j.matt.2020.10.021.
[84] R. Yang, L. Mei, Y. Fan, Q. Zhang, H.-G. Liao, J. Yang, J. Li, Z. Zeng, Fabrication of liquid cell for in situ transmission electron microscopy of electrochemical processes, Nat. Protoc. 18 (2023) 555–578, https://doi.org/10.1038/s41596-022-00762-y.
[85] J.-Y. Ye, Y.-X. Jiang, T. Sheng, S.-G. Sun, In-situ FTIR spectroscopic studies of electrocatalytic reactions and processes, Nano Energy 29 (2016) 414–427, https://doi.org/10.1016/j.nanoen.2016.06.023.
[86] M.M. Amaral, C.G. Real, V.Y. Yukuhiro, G. Doubek, P.S. Fernandez, G. Singh, H. Zanin, In situ and operando infrared spectroscopy of battery systems: progress and opportunities, J. Energy Chem. 81 (2023) 472–491, https://doi.org/10.1016/j.jechem.2023.02.036.
[87] K. Kanamura, S. Toriyama, S. Shiraishi, M. Ohashi, Z.-i. Takehara, Studies on electrochemical oxidation of non-aqueous electrolyte on the $LiCoO_2$ thin film

electrode, J. Energy Chem. 419 (1996) 77–84, https://doi.org/10.1016/S0022-0728(96)04862-0.
[88] G. Cherkashinin, M. Motzko, N. Schulz, T. Späth, W. Jaegermann, Electron spectroscopy study of Li[Ni,Co,Mn]O_2/electrolyte interface: electronic structure, interface composition, and device implications, Chem. Mater. 27 (2015) 2875–2887, https://doi.org/10.1021/cm5047534.
[89] C. Hogrefe, T. Waldmann, M. Hölzle, M. Wohlfahrt-Mehrens, Direct observation of internal short circuits by lithium dendrites in cross-sectional lithium-ion in situ full cells, J. Power Sources 556 (2023) 232391, https://doi.org/10.1016/j.jpowsour.2022.232391.
[90] T. Lombardo, F. Walther, C. Kern, Y. Moryson, T. Weintraut, A. Henss, M. Rohnke, ToF-SIMS in battery research: advantages, limitations, and best practices, J. Vac. Sci. Technol. A 41 (2023), https://doi.org/10.1116/6.0002850.